Reviewed Preprint
v1 • August 22, 2025
Not revised

Reviewed Preprint
v2 • May 6, 2026
Revised by authors

For correspondence:
hussain@iisc.ac.in

Competing interests: No competing interests declared

Funding: See page 18

Reviewing editor: Yogesh K Gupta, The University of Texas Health Science Center at San Antonio, United States

Structural insights into the recruitment of viral Type 2 IRES to ribosomal preinitiation complex for protein synthesis

Deepakash Das, Tanweer Hussain

Department of Developmental Biology and Genetics, Indian Institute of Science, Bengaluru, India

eLife Assessment

This manuscript offers **valuable** structural and mechanistic insights into the assembly of the Type II internal ribosome entry site (IRES) from encephalomyocarditis virus (EMCV) and the translation initiation complex, revealing a direct interaction between the IRES and the 40S ribosomal subunit. A **solid** experimental strategy, combining cryo-EM analysis, complementary biochemistry, and detailed structural comparisons, provides mechanistic insights into IRES-based translation initiation systems. This paper will attract researchers in cap-independent translation, host-pathogen interactions, and virology.

https://doi.org/10.7554/eLife.107788.2.sa4

Abstract

Picornaviruses employ internal ribosome entry sites (IRESs) in their genomic RNA to hijack the host's translational machinery. The picornavirus, Encephalomyocarditis virus, employs a type 2 IRES present in its 5'UTR and requires 43S ribosomal preinitiation complex (PIC), the central domain of eukaryotic initiation factor (eIF) 4G, eIF4A, and an essential ITAF (IRES trans-acting factor)-polypyrimidine tract binding protein 1 (PTB1) to form 48S PIC. In this study, we have used cryo-electron microscopy (cryo-EM) to determine the structure of EMCV IRES-bound mammalian 48S PIC in a scanning-arrested closed state at the start codon. The EMCV IRES domains contacts initiator tRNA ($tRNA_i$) and 40S head at the inter-subunit interface, which reveals an altogether unique mechanism used by viruses to capture host translational machinery for its protein synthesis. The $tRNA_i$ is held away from the 40S body in contrast to canonical cap-dependent translation while the domain I apical region of EMCV IRES mimics 28S rRNA of 60S to interact with 40S ribosomal head proteins-uS13 and uS19. The structural analysis account for numerous biochemical studies on Type 2 IRES and shows how Type 2 IRES interacts with 43S PIC to form 48S PIC. This study provides mechanistic insights for understanding EMCV IRES-mediated translation initiation, which could be extrapolated to other IRESs sharing similar motifs and factor requirements including type 1 viral IRESs.

Introduction

Eukaryotic translation initiation occurs in two different modes-Cap-dependent and Cap-independent. Cap-dependent translation initiation in eukaryotes can be divided into four major steps-(i) formation of 43S ribosomal PIC [40S subunit in complex with eIF1, eIF1A, eIF3, eIF5 and ternary complex (eIF2-GTP-$tRNA_i$)]; (ii) recruitment of 43S PIC to 5'end of capped mRNA, mediated by eIF4F complex (formed by eIF4E,eIF4G and eIF4A) yielding 48S complex (48S PIC); (iii) scanning of 5' untranslated region (UTR) of mRNA and start codon recognition; and (iv) joining of large 60S ribosomal subunit to form elongation-competent 80S ribosomal complex. Among these, major rate-limiting steps include-the regulation of available $tRNA_i$ as the ternary complex (eIF2.GTP.Met-$tRNA_i$) and recruitment of mRNA on 43S PIC (Jackson et al 2010; Brito Querido et al 2024).

Cryo-EM studies on eukaryotic canonical 48S PICs from yeast (Hussain et al 2014; Llácer et al 2015) to humans (Eliseev et al 2018; Simonetti et al 2020; Brito Querido et al 2020; Yi et al 2022; Brito Querido et al 2024; Petrychenko et al 2024) have revealed various interactions among the initiation factors, mRNA, and ribosome in scanning (P_{OUT} or open) state and scanning-arrested (P_{IN} or closed) states. In mammals, 48S PIC formation is mediated by the interaction of eIF3 and eIF4G (Villa et al 2013) and recent attempts to understand the mammalian canonical 48S PIC could capture interactions of eIF4 proteins (eIF4G and eIF4A) with eIF3 (Brito Querido et al 2020; Brito Querido et al 2024).

Alternatively, several positive strand RNA viruses use Internal Ribosome Entry Sites (IRESs), which are internal cis-acting sequences present in 5' UTR of mRNA that drive the assembly of translation initiation complex without the requirement of 7-methylguanosine cap (Martinez-Salas et al 2018), initially reported in picornaviruses such as poliovirus (PV) and encephalomyocarditis virus (EMCV) RNA genome (Jang et al 1988; Pelletier and Sonenberg, 1988; Trono et al 1988). As of 2020, the IRESbase database reported 1328 IRESs, out of which 554 were viral IRESs from 198 viruses (Zhao et al 2020). These RNA elements have unique secondary and tertiary structures, which allows them to hijack the host translational machinery and promote translation initiation internally by recruitment of host ribosome, canonical eIFs, and IRES trans acting factors (ITAFs) via multiple RNA–RNA and RNA–protein interactions (Lee et al 2017; Martinez-Salas et al 2018). The IRESs lack sequence homology and enfolds different structural organization, thus requiring different eIFs for the assembly of 48S PICs (Jackson et al 2010). The type 1 IRES (represented by PV) and type 2 IRES (EMCV) requires almost all eIFs, except eIF4E or N terminal of eIF4G for the formation of 48S PIC (Lozano and Martinez-Salas, 2015). However, initiation on the latter does not require scanning for start codon recognition (Kaminski et al 1994; Sweeney et al 2014). The type 3 IRES (Hepatitis C virus-HCV) does not require eIF4 factors or scanning for 48S PIC formation (Niepmann and Gerresheim 2020). The type 4 IRES (Cricket paralysis virus-CrPV intergenic IRES) initiates without the requirement of any eIFs and $tRNA_i$ (Johnson et al 2017). The HCV IRES and CrPV intergenic IRES directly interacts with host 40S ribosome, however they differ in their mechanism of attachment. Where, the CrPV IRES (type 4) mimics anticodon-codon interaction via pseudoknot 1 to bind with ribosome in an elongation-competent state (Petrov et al 2016; Fernández et al 2014) the HCV IRES (type 3) binds to the solvent side of 40S subunit by replacing eIF3 and directly interacts with expansion segment (ES7) of 18S rRNA and ribosomal proteins near mRNA exit channel, thus placing the initiation codon at the P-site (Hashem et al 2013; Niepmann and Gerresheim 2020; Brown et al 2022). While the structures of ribosome-bound type 4 (Spahn et al 2004; Fernández et al 2014; Muhs et al 2015; Murray et al 2016; *Pisareva et al 2018;* Acosta-Reyes et al 2019; *Abaena et al 2020*) and type 3 IRES (Spahn et al 2004; Boehringer et al 2005; Hashem et al 2013; Yamamoto et al 2014; Quade et al 2015; Yamamoto et al 2015; Yokoyama et al 2019; Brown et al 2022) have been determined, there is no structural information about Type 2 and Type 1 IRES and their mode of recruitment to 48S PIC.

The 5'UTR of EMCV, genera Cardiovirus and Picornaviridae family (International Committee on Taxonomy of Viruses Executive Committee, 2020) folds into various stem-loops numbered D-L, where domains H-L, followed by the initiation codon at the 834^{th} residue (~450 nucleotides in length) make a functional IRES moiety (Carocci et al 2012). It requires the core of 43S PIC, the central domain of eIF4G, eIF4A, and an essential ITAF-polypyrimidine tract binding protein 1 (PTB1), and the presence of eIF4B enhances 48S formation (Hellen and Wimmer 1995; Martinez-Salas et al 2018; Sweeney et al 2014). Functional characterization of these domains showed H, and I interact with 40S ribosomal subunit (Chamond et al 2014), and domain J-K recruits eIF4G, enhanced by eIF4A (Pestova et al 1996; Lomakin et al 2000). The structure of domain J-K-eIF4G1(HEAT1)-eIF4A revealed that positively charged patches on the eIF4G1-HEAT1 domain interact with two separated negatively charged clefts (in domains J and St) without perturbing its innate function of recruiting eIF4A (Imai et al 2016; Imai et al 2023). The binding sites for PTB1 were revealed to be dispersed, encompassing domains H to L (Kafasla et al 2009). These domains function as a single entity to form 48S PIC and any mutation in conserved IRES motifs can drastically affect the translation rates (Fernández-Miragall et al 2009; Fernández et al 2011).

For example, the RAAA and GNRA loop in the domain I of type 2 IRES are crucial for IRES activity (Robertson et al 1999), and the GNRA loop is also found in other IRES families such as type 1 (poliovirus) and type 5 (Aichi virus A) picornaviruses (Abdullah et al 2023). The inherent flexibility within the IRES domains provides a challenge for structural studies of full-length IRES and to capture IRES in the context of 48S PIC. EMCV IRES can independently interact with 40S subunit without any eIFs (Chamond et al 2014) and does not require scanning to recognize the start codon (Pestova et al 1996), unlike type 1 IRESs, which scan for the start codon (Sweeney et al 2014). Besides, EMCV IRES can form 48S PIC with HEAT1-eIF4G without the requirement of eIF4G residues 1015-1104 that are known to interact with eIF3 (Lomakin et al 2000). These residues are indispensable in case of canonical initiation on capped mRNAs and for type 1 IRESs (Villa et al 2013; Sweeney et al 2014). However, how EMCV IRES interacts with 40S subunit, or what molecular interactions are essential to form the EMCV IRES-48S PIC remains a question.

In this study, we have used pull-down assay to isolate EMCV IRES-bound 48S PIC from Rabbit Reticulocyte Lysate (RRL) and subjected the complex to cryo-electron microscopy (cryo-EM) analysis. The cryo-EM map of EMCV IRES-bound 48S PIC, henceforth mentioned as EMCV IRES-48S PIC, shows densities corresponding to EMCV IRES domains that reveal how EMCV IRES contacts the ternary complex and 40S head at the inter-subunit interface. The structural details presented here account for numerous biochemical studies that have been reported earlier on Type 2 IRES. Furthermore, the structural analysis suggests how Type 2 IRES would interact with 43S PIC to form 48S PIC. Importantly, the study reveals a unique strategy used by viral IRES to capture the host translational apparatus for making viral polypeptide.

Results

1. Overview and features of EMCV IRES-48S PIC

To isolate 48S PIC on EMCV IRES, we used a Talon affinity-based pull-down from nuclease-treated RRL. EMCV IRES RNA used harboured residues from 280 to 905 with AUG (start codon) at 834th position. PTB1 was recombinantly overexpressed with an N-terminal 6X His tag, followed by a 3C protease cleavage site. PTB1 was incubated with the IRES, followed by RRL addition, and 48S PIC was stalled using GMP-PnP. The complex was eluted from the Talon matrix employing 3C protease cleavage and pelleted (Sup. Fig. 1.1 A). The EMCV IRES-48S PIC was subsequently analysed by Cryo-EM. The processed data yielded 3 major classes-(i) 40S without any factors-Map A, (ii) 40S-IRES-$tRNA_i$-Map B, and (iii) 40S-IRES-ternary complex-Map B1, namely, EMCV IRES-48S PIC (Sup. Fig. 1.1 B). Map B and Map B1 have an overall resolution of 4.6 Å and 5.0 Å, respectively (Sup. Fig. 1.1 B). The core of 40S is at around 4.0 Å, and the local resolution across the maps was largely in the range of 4.0-8 Å (Sup. Figs. 1.2 A and B). Only the extreme tip of beak of 40S in Map B1 (Sup. Fig. 1.2 A) and ends of IRES and eIF2γ are around 12 Å in Map B2 (Sup. Figs 1.2 B).

The cryo-EM densities in EMCV IRES-48S PIC correspond to 40S, $tRNA_i$, eIF2α, eIF2γ, and RNA in the mRNA channel, along with an extra density connecting 40S ribosomal head to $tRNA_i$ (Fig. 1 A-B). However, it lacks distinct density for PTB1, eIF4G, eIF4A, and eIF3, and hence these factors are not modelled. Since nuclease-treated RRL lacked endogenous RNA, the presence of density for mRNA in the channel indicates trapping of EMCV IRES in 48S PIC. Also, the density connecting 40S head to $tRNA_i$ in Map B and B1 could be assigned to a double-stranded RNA structure found in EMCV IRES (Fig. 1 A-B).

Besides, an extra density is evident at the mRNA entry site, contacting 40S ribosomal proteins-uS3, eS10, and uS5 and h16 (Helix 16) of 18S rRNA (Sup. Fig. 1.2 C). In the human 48S PIC, this region positions eIF3g-RRM (RNA recognition motif) and downstream ORF (Sup. Fig.1.2 D) (Brito Querido et al 2020; Brito Querido et al 2024). We anticipate that this extra density in EMCV IRES-48S PIC could be contributed by downstream ORF; however, it's difficult to assign it to eIF3g-RRM due to the lack of eIF3 (core/peripheral) density. Furthermore, our recent study on interaction of yeast eIF4B with 40S ribosome suggested occupancy of eIF4B (N terminal-RRM) in the same region (Datey et al 2025), which opens up the possibility of mammalian eIF4B-NT-RRM to bind to this region in the absence of eIF3, although in the human 48S PIC eIF4B was tentatively positioned

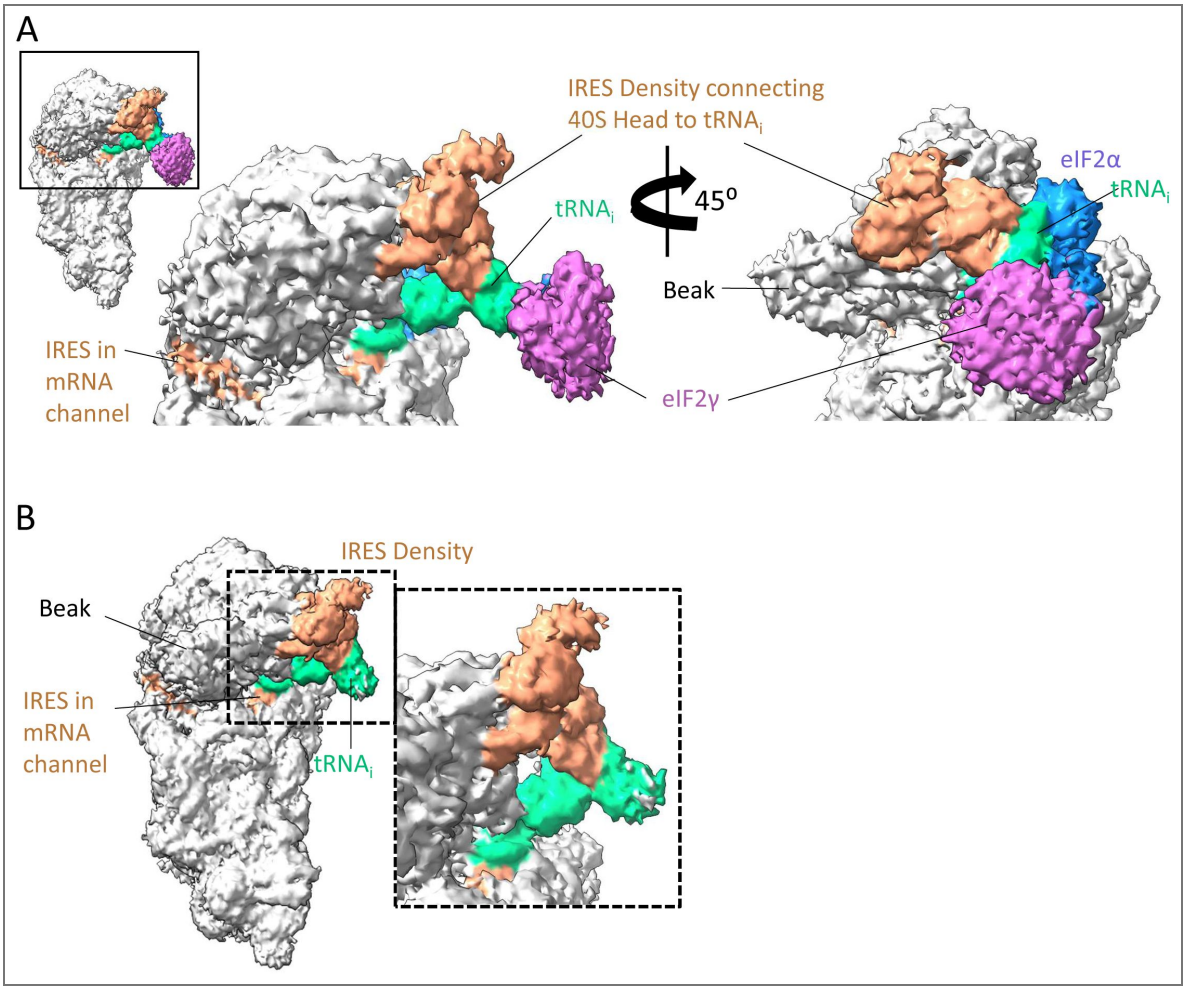

Figure 1.

(A) Different views of EMCV IRES-48S PIC (Map B1) by 45º rotation along one axis. The map shows densities assigned to 40S ribosome, RNA (in channel), ternary complex and IRES density at the inter-subunit region of head. **(B)** View of Map B and zoomed view of densities corresponding to IRES and $tRNA_i$.

slightly away from this location (Brito Querido et al 2024). An interesting possibility could be positioning one of the RRM domains of PTB1 bound to UCUUU sequence of 18S rRNA (PTB1 can bind to UCUUU sequence - Maris et al 2020) present at the tip of h16 (528-532 nucleotides) of 18S rRNA. An extra density in the same position is also present in Map A (40S without EMCV IRES or factors-Sup. Fig. 1.2 E) as well, and PTB1 was used as a bait for the pull-down; therefore, this density may be contributed by PTB1-RRM interacting with h16 of 18S rRNA.

2. The EMCV IRES-48S PIC is trapped in a closed conformation

In EMCV IRES, A-834-U-835-G-836 (AUG-834) forms the start codon (Kaminski et al 1994; Hellen and Wimmer 1995; Pestova et al 1996). Previous experiments based on toeprints of EMCV IRES-48S PIC assembly suggested A-826-U-827-G-828 (AUG-826) as the codon where 48S PIC can assemble, and AUG-834 as the start codon (Pestova et al 1996). Furthermore, the intensity of the toeprint at AUG-834 was much higher than at AUG-826 (Pestova et al 1996; Sweeney et al 2014). Also, AUG-834 is present in a Kozak context (CRCCaugG; R is a purine) (Kozak 1989), where the -3 position is A-831 and +4 is G-837 (Sup. Fig. 2 D), whereas AUG-826 is present in a poor Kozak context. In this work, the EMCV IRES construct used has both AUG-826 and AUG-834. Based on the above-mentioned reports, poor and strong Kozak context of AUG-826 and AUG-834, respectively, and placement of AUG-834 at the P site in EMCV IRES-40S binary complex (Chamond et al 2014), we reason AUG-834 to base-pair with the anticodon in EMCV IRES-48S PIC (Fig. 2 A), and the flanking nucleotide residues were added as per the sequence (Sup. Fig. 2 D). The recognition of the start codon at the P-site by $tRNA_i$ leads to accommodation of ternary complex, and 48S PIC adopts a P_{IN} state in contrast to P_{OUT} state observed during scanning (Llácer et al 2015; Llácer et al 2021; Yi et al 2022; Petrychenko et al 2024). A distinct difference of ~7.0 Å could be seen by comparing the $tRNA_i$ position of EMCV IRES-48S PIC with that in the open state (Fig. 2 B), depicting a P_{IN} state of $tRNA_i$. The entrapment of the start codon in the P-site also evokes closure of the mRNA latch formed by 18S rRNA helices-h34 of 40S head and h18 of body (Hussain et al 2014; Llácer et al 2015; Hinnebusch 2017). The h34 of 18S rRNA of EMCV IRES-48S PIC is shifted by 9 Å as compared to the human canonical open state 48S PIC (PDB Id-7QP6, Yi et al 2022). This conformation of 18S rRNA correlates well with that of closed 48S PIC (PDB Id-7QP7, Yi et al 2022), suggesting EMCV IRES-48S PIC was captured in a closed state (Fig. 1 C). This closed conformation locks the mRNA in the channel formed within 40S head and body. On the other hand, the conformation of 18S rRNA in Map A (40S ribosome without initiation factors) shows an open state (Sup. Fig. 2 E). The transition from open (PDB Id-7QP6) to closed states (PDB Id-7QP7) structures is also accompanied by an upward shift of N terminal domain of eS17 (connecting the head to body) by ~10 Å (Yi et al 2022). The EMCV IRES-48S PIC structure correlates with the conformation of eS17 in the human 48S-closed PIC, that is, eS17 N-terminal helix associated with the ribosomal head shifts upward by ~10 Å, keeping C-terminal domain position constant (Fig. 2 D; Sup. Fig. 2 F).

3. The IRES density connecting 40S head to $tRNA_i$ is contributed by the I domain apical part

In EMCV IRES-48S PIC complex, we observed a density, likely for double-stranded RNA, connecting 40S head to the $tRNA_i$ elbow region (Fig. 3 A). The extra density interacts with the elbow region and acceptor stem of $tRNA_i$ and ribosomal proteins-uS19 (RPS15) and uS13 (RPS18) (Nomenclature - Ban et al 2014). The EMCV IRES contains 4 major stem-loops (H-L) in the functional IRES region (Fig. 3 B) (Hellen and Wimmer 1995). Among these, domains H and I have been shown to interact with 40S (Chamond et al 2014) and mutations of conserved residues in these domains severely compromise translation on EMCV IRES (López de Quinto and Martínez-Salas 1997; Hellen and Wimmer 1995). Moreover, incubation of Foot and Mouth Disease Virus (FMDV) IRES, an EMCV-like type 2 IRES, with 40S ribosomes has shown a decrease in SHAPE reactivity in its domain 3 apex (Lozano et al 2018), which corresponds to EMCV IRES domain I apex. We reasoned that domains H and I may contribute to the double-stranded RNA density emanating from 40S head. The density architecture (Fig. 3 C) could be interpreted as a long main stem (S1)

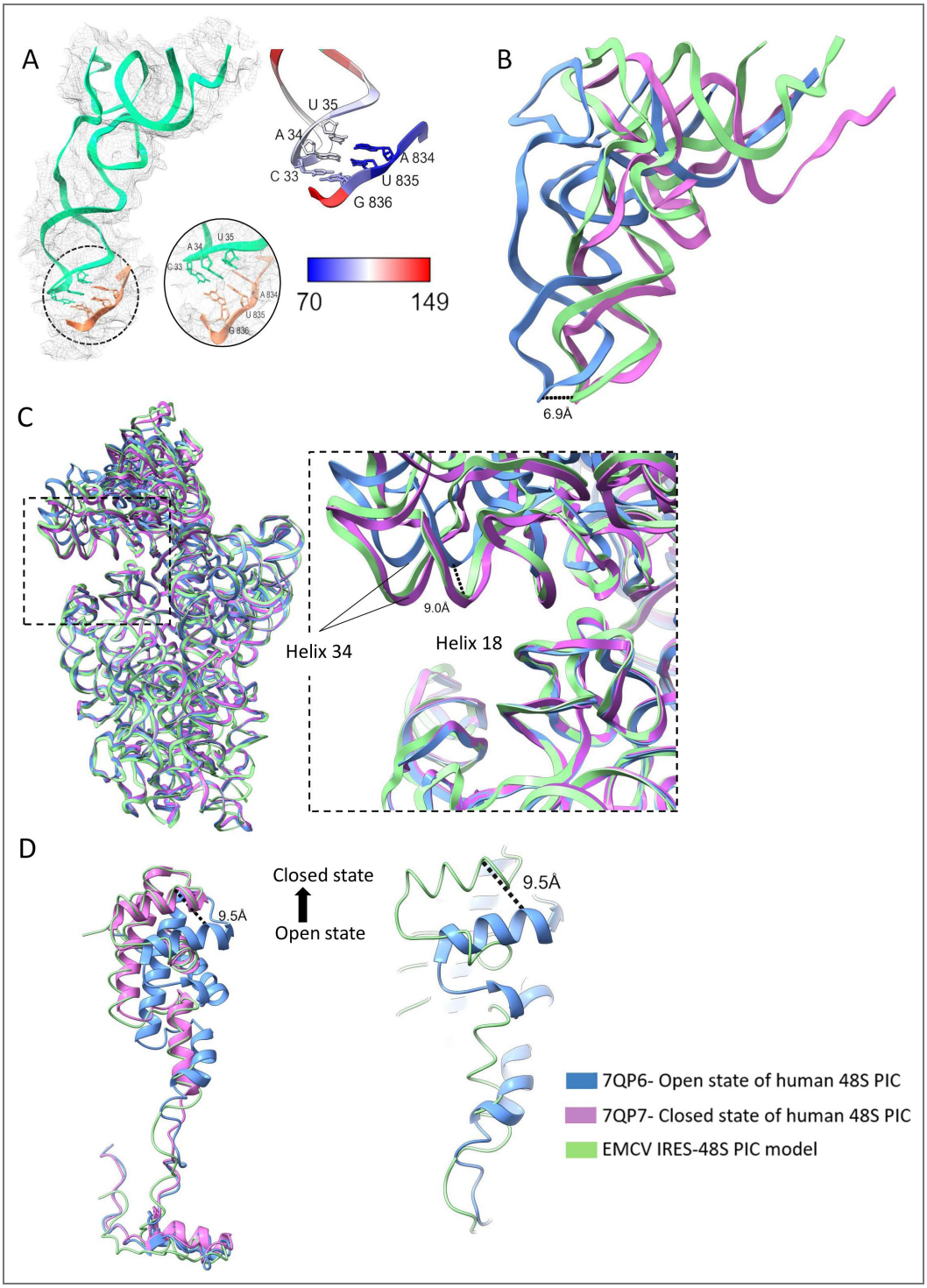

Figure 2.

(A) Fitting of $tRNA_i$-base paired to start codon AUG (left). Zoomed view of codon-anticodon interaction (middle), and B-factor for codon-anticodon interaction (right). **(B)** The $tRNA_i$ in EMCV IRES-48S PIC is in P_{IN} state similar to that in human 48S PIC P_{IN} state (PDB Id-7QP7) and its anticodon shows ~7 Å shift as compared to human 48S PIC open state (PDB Id-7QP6). **(C)** Comparison of ribosomal conformation (18S rRNA) of EMCV IRES 48S PIC with Human open and closed state (PDB Id-7QP6 and 7QP7, respectively). Focusing on the entry site and the helices governing latch conformation-Helix 34 moves toward helix 18 by 9 Å. **(D)** Movement of eS17 in open and closed states of ribosome. Zoomed view of comparison between eS17 in EMCV IRES 48S PIC and Human 48S PIC open state-showing an upward shift of the N-terminal domain by ~10 Å.

extending away from 40S where the base is anchored to the ribosome by two branches (B1 and B2), and to $tRNA_i$ by one branch (B3), further divided into two sub-branches (B3a and B3b). Visualizing the IRES RNAfold determined-secondary structure (Fig. 3 D-which correlates with the experimental structure proposed in Duke et al 1992), this architecture could be contributed by the apical part of domain I.

To determine the tertiary structure of the domain I apex, the IRES region from nucleotide 507-619 was modelled using Alphafold3 (Sup. Fig. 3.1 A). The model was decomposed and reconstructed based on the best-fit in the obtained density for the IRES using Chimera and Coot (Sup. Fig. 3.1 A). The final model was generated after multiple rounds of geometry correction and real space refinements (Fig. 3 E). The final model holds a correlation coefficient of 0.8 with respect to the map (Sup. Fig. 3.1 B), where B1 is AAG loop, B2 is CAAA loop, B3a-GCGA loop, B3b-C rich loop1, and S1 is the major double-stranded stem of domain I. The B-factor of the modelled IRES largely ranges from 124 to 200 (Sup. Fig. 3.1 C). To check the possibility of other IRES domains that might contribute to the extra density, Alphafold3 was used to predict the tertiary structure of isolated EMCV IRES domains (Sup. Fig. 3.2 A-J), using sequences as shown in Sup. Table 1. The predicted tertiary structure of domain H or experimental models of domains D to F did not fit in the observed IRES density (Sup. Fig. 3.2 K-L). The domain J-K adopts a Y-shaped structure, and placement of its cryo-EM (PDB Id-8HUJ) or NMR (PDB Id-2NBX) structure in the density would clash with 40S (Sup. Fig. 3.2 M). Moreover, in context to EMCV IRES-48S PIC, domain J-K binds eIF4G and the location of eIF4G has been mapped close to ES6 of 18S rRNA, located near the left foot 40S ribosome (Yu et al 2011). The domain I apex model in EMCV IRES-48S PIC shows the RAAA and AAG motif contacts uS19 and uS13, and the GNRA loop with $tRNA_i$ (Fig. 4 A). In addition, incubation of EMCV IRES with rabbit reticulocyte lysate (RRL) protected domain I apex regions, including the CAAA loop in the SHAPE reactivity profile (Maloney and Joseph, 2024). These interactions with 40S head and $tRNA_i$ could be facilitated by the long length and flexible nature of domain I.

4. The interaction of domain I of EMCV IRES with ribosomal proteins and initiator tRNA

The domain I is the longest domain in EMCV IRES, which harbours important motifs such as GNRA, RAAA, and C rich, crucial for IRES activity (Roberts and Belsham, 1997; Fernández-Miragall and Martínez-Salas 2003) and conserved across all cardioviruses (Hellen and Wimmer 1995). We mutated the GNRA loop and RAAA loop in EMCV IRES and checked for luciferase activity using a firefly *Luciferase* reporter downstream of the wild-type and mutant IRESs. We found a drastic reduction in the luciferase activity in the mutants as compared to that of the wild-type (Sup. Fig. 4 A), which correlates with previous studies that showed the importance of these motifs in regulating IRES activity (Roberts and Belsham, 1997; López de Quinto and Martínez-Salas, 1997; Robertson et al 1999; Fernández-Miragall and Martínez-Salas 2003). Among these, the CAAA and AAG motifs share potential contact sites with uS13 and uS19. The alpha helix (100-117 residues) of uS13 contacts the IRES element at the B3 stem (connecting the GNRA loop to RAAA loop) (Fig. 4 B). uS19 contacts the IRES majorly at its CAAA motif through multiple sites involving N-terminal residues, residues-67 to 75, and C-terminal-102 to 124 (Fig. 4 C). These regions of uS13 and uS19 are rich in basic residues, which might interact with the negatively charged backbone of the IRES element (Fig. 4 B-C). The role of uS13 and uS19 also involves the formation of inter-subunit bridges during 60S joining to form elongation-competent 80S complexes. uS13 interacts with uL5 (RPL11) and uS19 with helix 38 or h38 (1748-1778, in humans) in 28S rRNA to form inter-subunit bridges-B1b/c and B1a, respectively (Sup. Fig. 4 B) (Ben-Shem et al 2011; Bowen et al 2015; Khatter et al 2015). These interactions are dynamic owing to ribosomal subunit rotation and swivelling during 80S ribosomal translocation states (Khatter et al 2015).

On superimposition of 80S ribosomal structure to EMCV IRES-48S PIC model, the IRES density clashes with the position of uL5 and h38 of 28S rRNA (Sup. Fig. 4 C), suggesting repositioning of IRES domain from 40S head during 48S to 80S transition. Interestingly, the h38 residues interacting

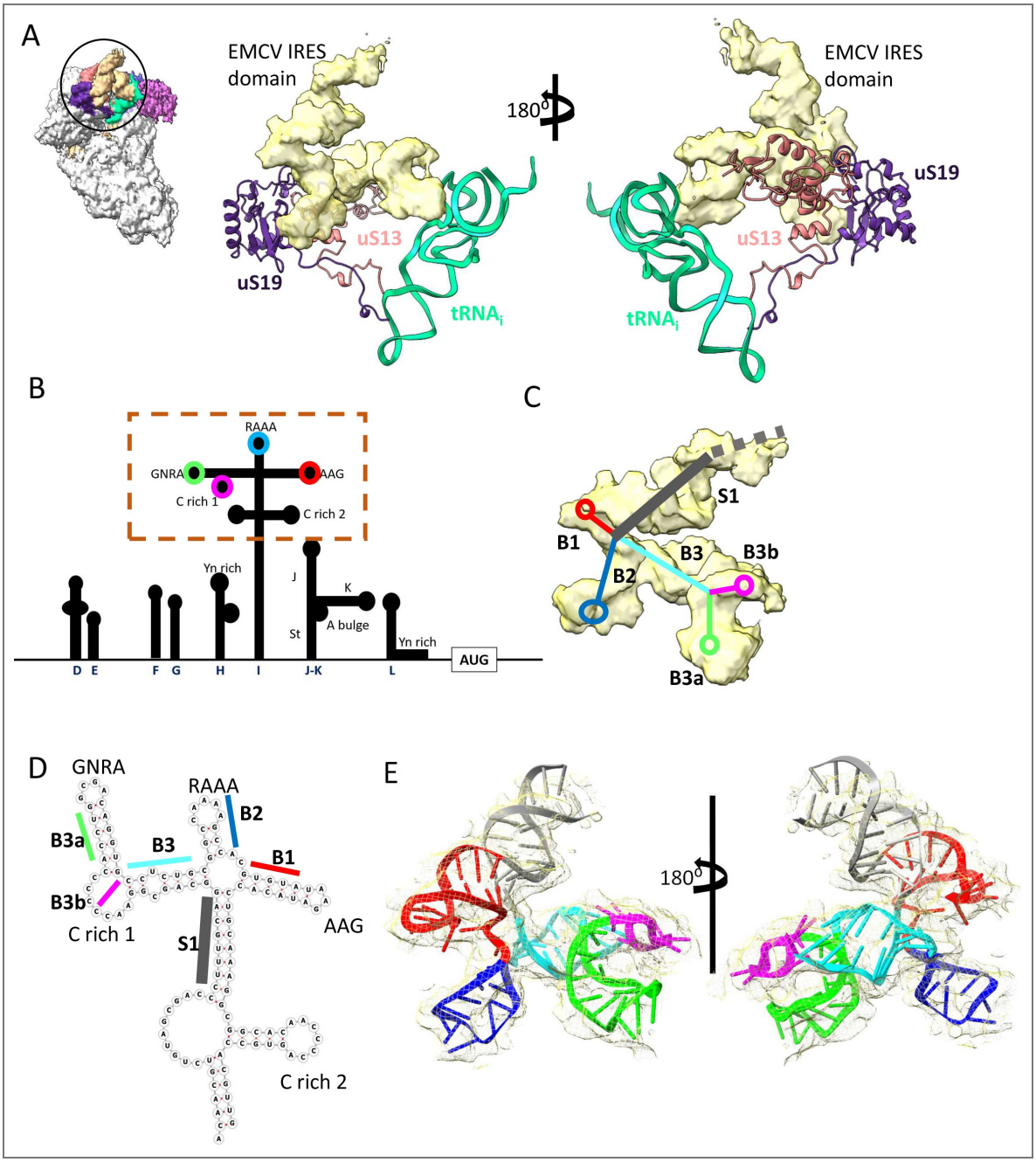

Figure 3.

(A) Extra density connecting the head of 40S to $tRNA_i$ elbow region is contributed by EMCV IRES RNA in Map B1. Rotated views of RNA density showing its connection to the 40S head via uS13 and uS19 and to $tRNA_i$ via its elbow region. **(B)** Organization of EMCV IRES domains from D-L, where H-L makes the functional IRES moiety (Hellen and Wimmer et al 1995). **(C)** Deciphering the architecture of the obtained IRES density. The density could be interpreted as a long main stem (S1) extending away from the ribosome, where the base is anchored to the ribosome by two branches (B1 and B2), and to $tRNA_i$ by one branch (B3), further divided into two sub-branches (B3a and B3b). **(D)** Secondary structure of apical region of domain I (made using RNAfold) marking the Stem and branches, along with imported loops. **(E)** Fitting of domain I apex in the density (Rotated views). The sub-domains are coloured as proposed in Fig 3C-D.

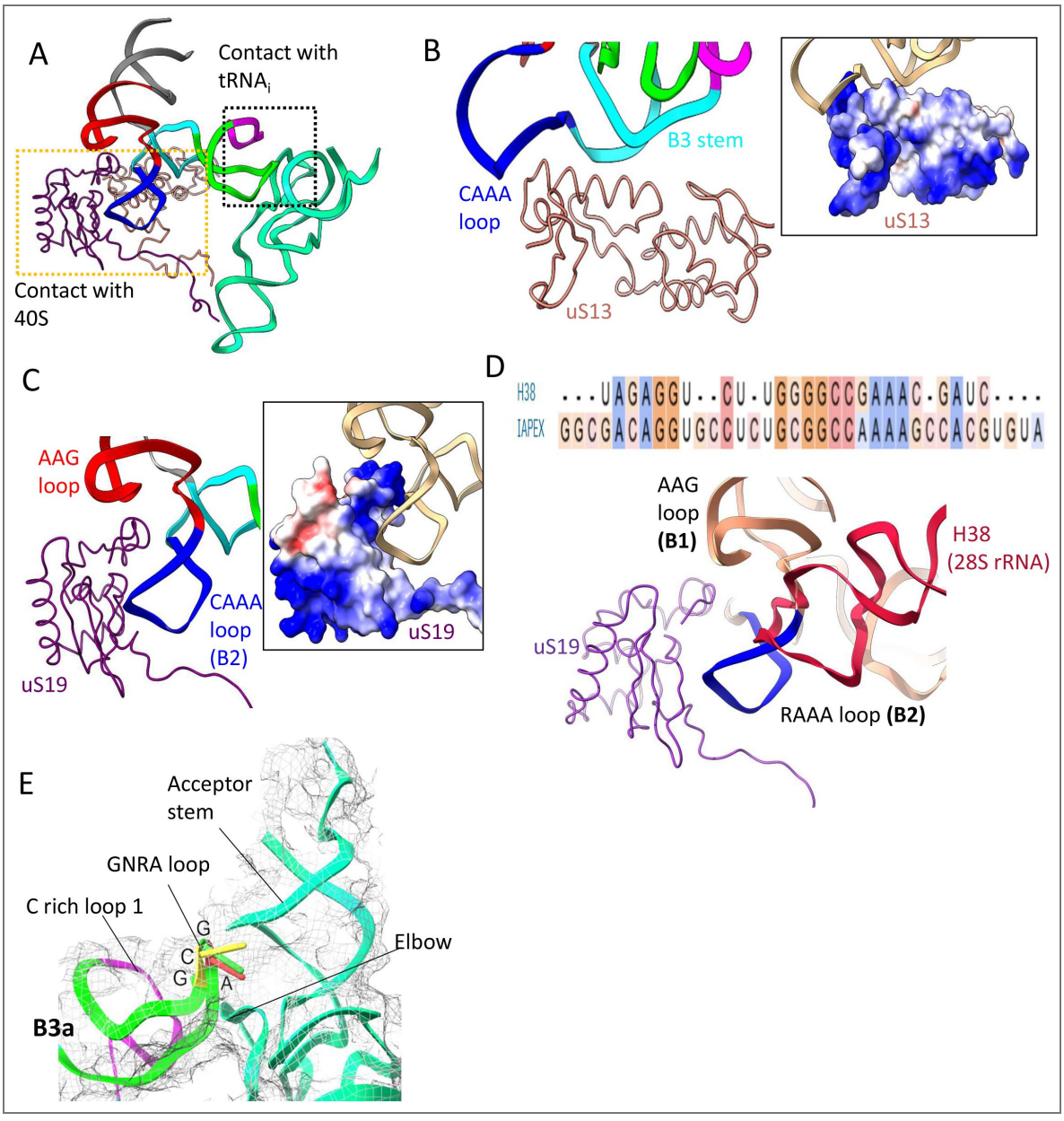

Figure 4.

(A) Model showing connections of domain I apex with uS13, uS19, and $tRNA_i$. **(B)** uS13 interacts with B3 branch or sub-domain of IRES via its alpha helix (100-117 residues). **(C)** Multiple point of contacts between uS19 and domain I motifs-RAAA and AAG. The electrostatic potential map of uS19 suggests that EMCV IRES interacts via ionic interactions with its phosphate backbone. **(D)** Sequence alignment of h38 with domain I apex of EMCV IRES showing sequence identity. Overlapping of uS19 from 80S (PDB Id-4UG0) and EMCV IRES-48S PIC show that the interaction of uS19 with EMCV IRES is similar to interaction with that of h38. **(E)** The fit of GNRA or GCGA stem and its contact with $tRNA_i$ at the elbow region and acceptor stem.

with uS19 shares considerable similarity in sequence to I domain apex in the EMCV IRES (Fig. 4D), suggesting the domain I apex of EMCV IRES could mimic h38 (60S)-40S interaction (Fig. 4D). The similarity of h38 with the domain I residues provides additional support for annotation of domain I apex in the density.

The GCGA (GNRA motif-where N is any nucleotide and R is a purine) is known for long-range RNA-RNA interactions, widespread in ribosomal RNA and in some catalytic RNAs. It forms a characteristic U-turn structure (Fiore and Nesbitt 2013) and interacts with minor grooves of helical RNA elements (Sup. Fig. 4 D - Reiter et al 2010). A single point mutation within this tetraloop (GCGA to GCGC) severely reduced the IRES activity, suggesting its essential for IRES activity (Roberts and Belsham, 1997; Fernández-Miragall and Martínez-Salas 2003). The density extending from the elbow region of $tRNA_i$ could fit in the characteristic U-turn, adopted by conventional GNRA motifs. In EMCV IRES, the GNRA motif is represented by GCGA loop, preceded by a C-rich region and in close contact with the $tRNA_i$ elbow and acceptor stem (Fig. 4 E). Thus, we infer that EMCV IRES interacts with $tRNA_i$ by virtue of its GCGA loop.

5. The position of eIF2-ternary complex is shifted towards 40S head in EMCV IRES-48S PIC in contrast to canonical 48S PIC

We could fit eIF2α and eIF2γ in their respective densities in Map B1 (Fig. 5 A). Focussed classification or refinement did not yield any distinct density corresponding to the position of eIF2β, probably due to the flexibility associated with repositioning of eIF2β during transition from open to closed complexes (Llácer et al 2015; Llácer et al 2021; Yi et al 2022; Petrychenko et al 2024). Previous reports on EMCV IRES suggested its direct interaction with eIF2 (Scheper et al 1991; Scheper et al 1994) and inactivation of eIF2 compromises EMCV IRES-mediated translation (Welnowska et al 2011; Kwon et al 2017), indicating EMCV IRES's dependence on the canonical ternary complex. Here, we observe a direct interaction of EMCV IRES with ternary complex via $tRNA_i$, a feature not observed in previously determined HCV (Yamamoto et al 2014; Yamamoto et al 2015; Brown et al 2022) and CrPV IRES-bound ribosomal structures (*Pisareva et al 2018*; Acosta-Reyes et al 2019).

As found in canonical 48S PICs (Hashem et al 2013; Brito Querido et al 2024; Petrychenko et al 2024), eIF2α-domain 1 is in close contact with ribosomal protein-uS7, and domain 2 with $tRNA_i$ elbow and domain 3 with eIF2γ in EMCV IRES-48S PIC. The position of eIF2γ and eIF2α-domain 3 (D3) is distinct from mammalian 48S-closed PICs (PDB Id-6YAN and 7QP7) as we could observe a shift by ~10 Å towards the head of 40S on superimposing the 18S rRNA from EMCV IRES 48S PIC and mammalian late-stage 48S PIC (Fig. 5 B). The ternary complex is flexible, and it moves away from ribosomal head towards the body on recognition of authentic start codon as studied in yeast (Villamayor-Belinchón et al 2024) and human (Petrychenko et al 2024). This opposite directional shift of the ternary complex in the EMCV IRES-48S PIC is evident in $tRNA_i$ acceptor stem as well (Fig. 5 C). This shift could be due to the rigid stem B3 (consisting G-C base pairs), connecting 40S head to GNRA loop, which interacts with the $tRNA_i$ at its elbow and acceptor arm, and the association of eIF2α-D3 and eIF2γ with the acceptor arm of $tRNA_i$ orchestrated with the conformational change.

During the transition of 48S PIC to 80S elongation-competent complex, there are major changes in the conformation of $tRNA_i$ due to the joining of eIF5B, and release of eIF2 (Petrychenko et al 2024). This joining event of eIF5B positions the $tRNA_i$ elbow and acceptor stem towards the 40S body to aid 60S ribosomal subunit joining (Petrychenko et al 2024). However, in the context of EMCV IRES-48S PIC, we have seen the positioning of $tRNA_i$ elbow and acceptor stem towards the 40S head, away from the body (Fig. 5 C). On superimposing the human 48S PIC structure (before 60S joining), 48S-5 (PDB Id-8PJ5-Petrychenko et al 2024), we could see that $tRNA_i$ in EMCV IRES-48S PIC is away from the canonical $tRNA_i$ position (in contact with eIF5B) (Fig. 5 D). Therefore, we anticipate a change in $tRNA_i$ conformation during eIF5B joining and eIF2 release. Furthermore, the IRES (domain I) interacting with the $tRNA_i$ elbow needs to be displaced from the position to facilitate the interaction of $tRNA_i$ with eIF5Band this rearrangement would also aid in 60S joining and avoid steric clash with the IRES domain I.

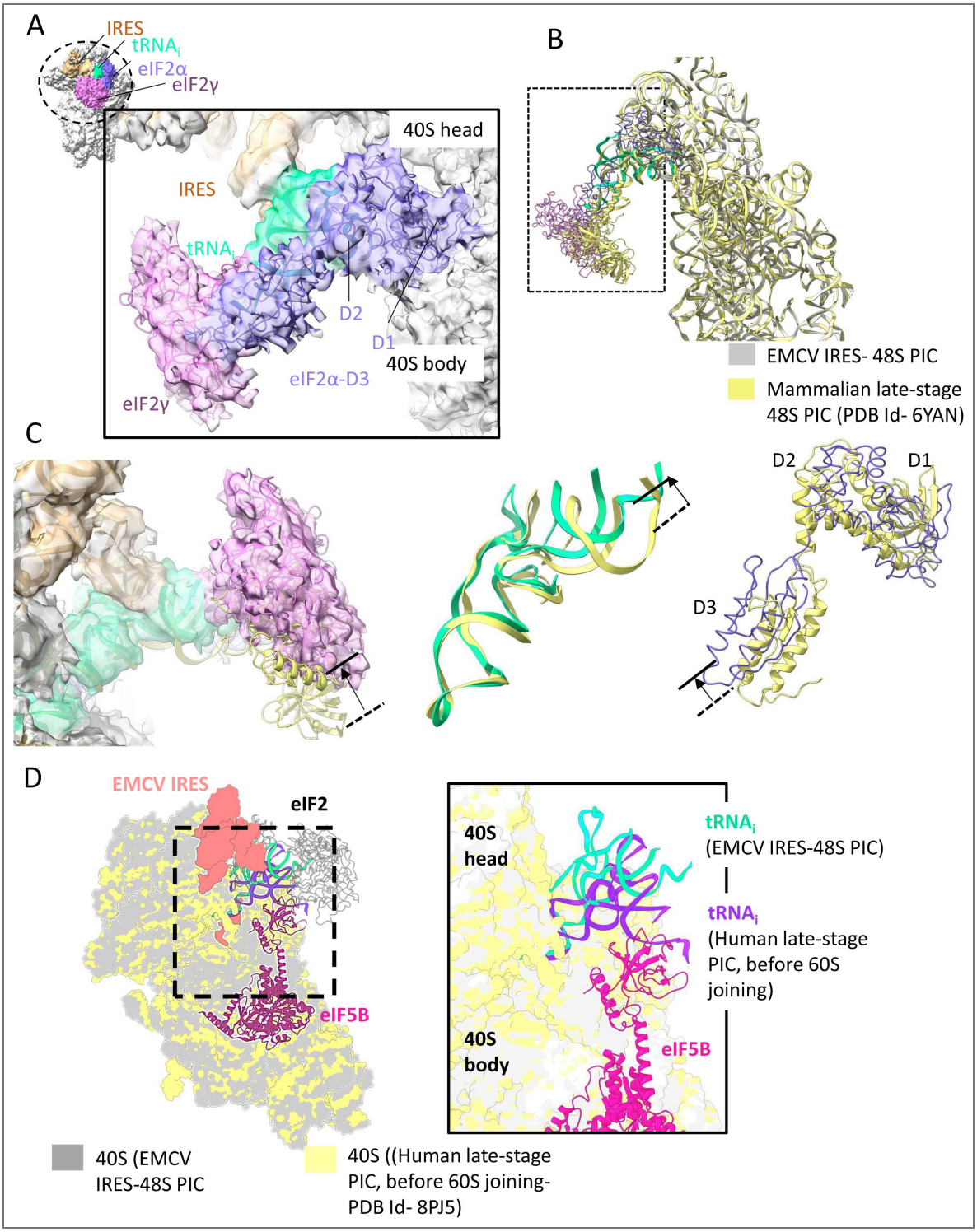

Figure 5.

(A) Inter-subunit view of EMCV IRES 48S PIC showing position for ternary complex on map. Fitting of eIF2α and eIF2γ in its corresponding density in Map B1. **(B)** Overlapping EMCV IRES 48S PIC on mammalian late-stage 48S PIC (PDB Id-6YAN), indicates a shift in position of eIF2γ towards 40S head. **(C)** Zoomed view showing the positions of eIF2γ, tRNAi, and eIF2α in the EMCV IRES 48S PIC relative to those in the mammalian late-stage 48S PIC (PDB ID 6YAN). The black arrow indicates the shift in position. **(D)** Superimposition of the EMCV IRES-48S PIC on the human late-stage 48S PIC (before 60S joining; PDB Id-8PJ5), showing the conformation of $tRNA_i$ in association with eIF2 and IRES and $tRNA_i$ with eIF5B in the canonical context, respectively. (right) Zoomed view of $tRNA_i$ conformation in both complexes.

Discussion

The mechanism of IRES recruitment on 40S ribosome varies considerably among different types of IRESs. CrPV intergenic IRES binds to 40S ribosome by mimicking tRNA-mRNA interaction with the help of pseudoknot 1 (Petrov et al 2016; Fernández et al 2014; Murray et al 2016; Acosta-Reyes et al 2019), whereas HCV IRESs associates with the solvent side of 40S body by replacing eIF3 with its domain 3 (Spahn et al. 2004; Hashem et al 2013; Niepmann and Gerresheim 2020; Brown et al 2022). In this study, we capture EMCV IRES in 48S PIC context, interacting with 40S ribosomal head and $tRNA_i$. Model building suggests that domain I of EMCV IRES interacts with 40S ribosome head and $tRNA_i$ elbow stem (Fig. 6 A). The similarity in the sequence of h38 of 28S rRNA with the domain I and its ability to interact with uS19-N terminal via RAAA motif (Khatter et al 2015) suggests a mimicry mechanism adopted by EMCV IRES for its recruitment to the ribosome. Moreover, the conservation of domain I apex sequence and motifs (RAAA, AAG loop, C-rich and GNRA) across Cardioviruses-Theiler's murine Encephalitis virus (TMEV), Vilyuisk human encephalomyelitis virus (VHEV), Theiler's-like rat virus (TRV) and Saffold viruses 1 and 2 (SAFV-1 and SAFV-2) and Apthoviruses (AAG loop is replaced by ACG loop)-Foot and mouth disease virus (Hellen and Wimmer 1995; Liang et al 2008) suggests that these IRESs might adopt similar strategies for 48S formation (Fig. 6 B-C). Like EMCV IRES, the type 1 IRES (Poliovirus, Coxsackie virus, etc.) also harbours the GNRA loop, preceded by a C-rich loop at its longest domain, known for long-range RNA-RNA interactions. The segment harbouring GNRA loop is highly conserved across the type 1 family of IRESs (Kim et al 2015). The domain I of EMCV IRES is similar to domain IV of polioviral IRES or other type 1 IRESs in terms of length, secondary structure, and conserved motifs (GNRA, C-rich) positioning (Fig. 6 C). Therefore, we anticipate a similar interaction of domain IV (in type 1 IRES class) with $tRNA_i$. Also, this interaction of IRES with $tRNA_i$ could be a strategy by which these IRESs can sequester the $tRNA_i$ pool in the cell, rendering them unavailable for capped cellular mRNAs. During the revision of this work, a preprint reported a structure of polioviral IRES-48S PIC (Velazquez et al 2025), which shows that domain IV apex (similar to domain I apex in EMCV IRES) interacts with uS13 and uS19, and the GNRA loop directly interacts with $tRNA_i$ during start codon recognition (Velazquez et al 2025) as observed in EMCV IRES-48S PIC. Similarly, the Aichi viral IRES (type 5-Abdullah et al 2023) harbours a GNRA loop in its longest domain, which is domain J. Deletion of the GNRA loop compromises the IRES activity; however, substitution mutations in this region either elevate the IRES activity or it remains unaltered (Yu et al 2011). We hypothesize that Aichiviral IRES might use this motif to mediate long-range interactions with tRNAi, similar to type 1 and type 2 IRESs, as all these IRESs require eIF2-ternary complex for the formation of 48S PIC.

The EMCV IRES does not require scanning, and the start codon (A-834) is directly placed in the P site, which would eventually place the domain L at the mRNA exit site, preceded by domain J-K that interacts with eIF4G-eIF4A (Fig. 6 A). Earlier, biochemical studies suggested eIF4G to be positioned close to ES6 of 18S rRNA in EMCV IRES-bound 48S PIC (Yu et al 2011). The human 48S PIC with a 5' capped mRNA showed a similar location for eIF4G, that is at the mRNA exit site contacting eIF3 (Brito Querido et al 2020; Brito Querido et al 2024). Locating eIF4F has been challenging due to the inherent flexibility associated with the eIF4F complex on mRNA and requires association with eIF3 in canonical 48S context (Brito Querido et al 2020; Brito Querido et al 2024). However, the canonical eIF3-eIF4G interaction (Villa et al 2013) is dispensable for EMCV IRES-48S PIC formation (Lomakin et al 2000; Sweeney et al 2014), and no density for eIF3 was observed even after focused classification. However, after the initial submission of this work, a preprint reported a structure of reconstituted EMCV IRES-48S PIC where eIF3 is present at the canonical position (*Bhattarcharjee et al 2025*). This position of eIF3 suggests the possibility that eIF4G-eIF4A proteins could be placed similarly to the canonical eIF3-eIF4G-eIF4A position (Brito Querido et al 2024) in context to EMCV IRES-48S PIC. Thus, placing eIF4G-domain J-K close to ES6 of 40S ribosome, which coincides with the previous hydroxyl radical cleavage assay (Yu et al 2011). In addition to initiation factors, the ITAF-PTB1 serves as an essential ITAF for 48S PIC formation on EMCV IRES, but the obtained map shows no distinct density to PTB1. PTB1 binds to the base of domains H and I, and domain K loop (Kafasla et al 2009; Dorn et al 2023), and the

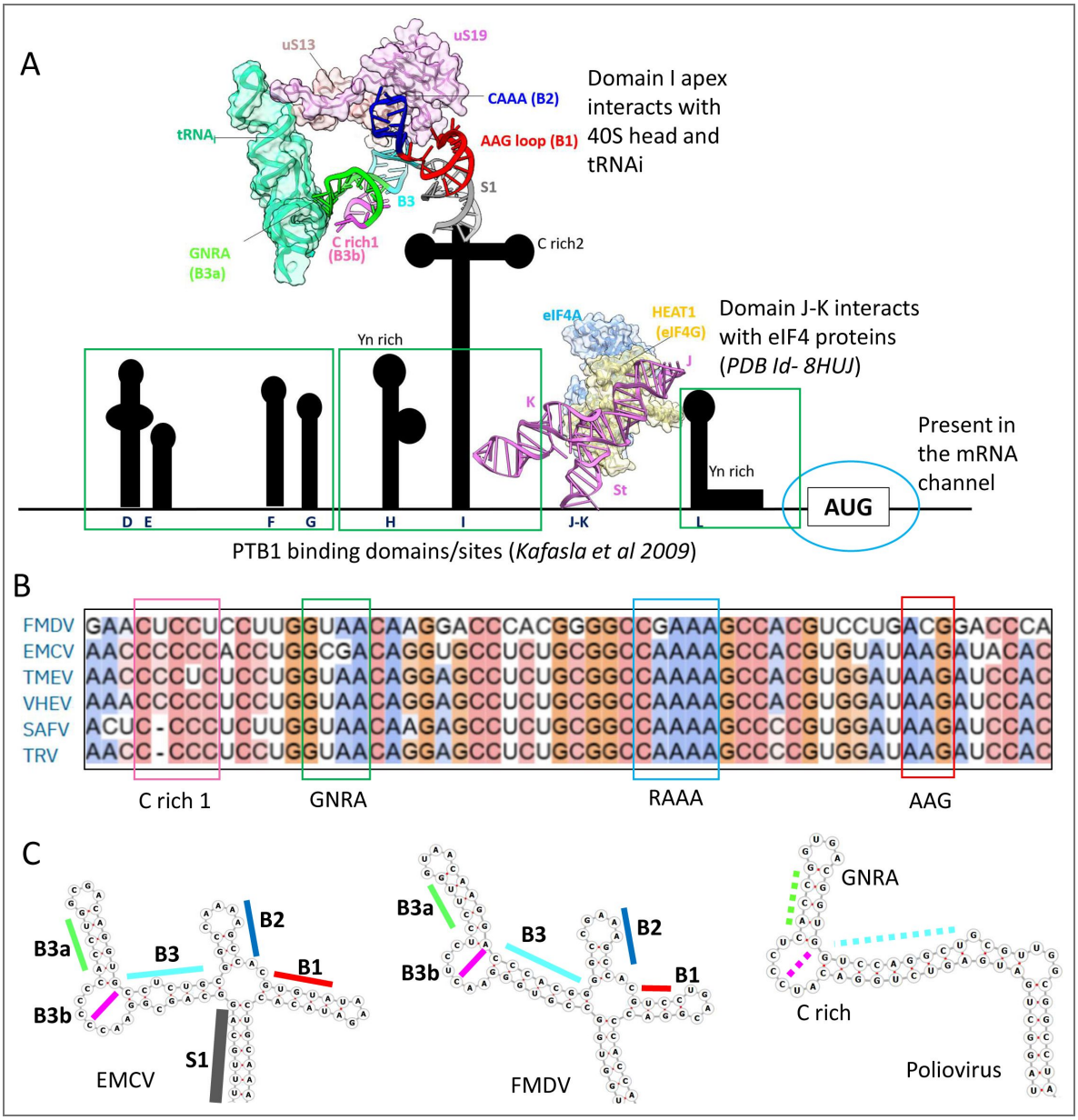

Figure 6.

(A) EMCV IRES secondary structure depicting the role of binding partners for each domain in context to translation initiation. The known tertiary structure of EMCV IRES and its binding partners are depicted. The domains responsible for binding PTB1 are boxed. **(B)** Conservation of domain I apex sequence and secondary structure across type 2 IRES family. **(C)** Comparison of secondary structure of EMCV and FMDV IRES to that of Polioviral IRES (type 1).

flexibility associated with these domains might have hindered capturing of PTB1 in the reported 48S complex (Fig. 6 A). However, the unassigned extra density at the mRNA entry site could be contributed by PTB1-RRM interacting with 18S rRNA, as discussed previously.

The structural studies on type 2 IRESs have been limited due to their flexible nature. In the cryo-EM map and structural analysis presented here, we could capture a part of EMCV IRES in 48S context (Fig. 6 A) and fetch a significant understanding of ribosomal recruitment by EMCV IRES and 48S PIC formation. As mentioned above, the cryo-EM map of reconstituted EMCV IRES-48S PIC (*Bhattarcharjee et al 2025*) show similar findings, where the density for the apical portion of domain I of the IRES is only observed and it interacts with uS13 and uS19 on 40S ribosome, and $tRNA_i$. A higher resolution of the reconstituted EMCV IRES-48S PIC (3.2 Å) helped the authors to identify interactions of individual IRES nucleotides with their binding partners (*Bhattarcharjee et al 2025*). In future, the entrapment of additional factors would significantly provide more insights into EMCV IRES 48S PIC. The conservation of secondary structures and motifs such as GNRA within the picornaviruses (type 1, 2, and Aichiviral IRESs) suggests common strategies of interaction in the context of 48S PICs in the Picornaviridae family.

Materials and Methods

1. Plasmid constructs and Molecular Cloning

EMCV IRES 905 was obtained from EMCV-L plasmid-EMCV IRES (nt 280–905) into pCR2.1 and inserted in pcDNA3.1 using BamHI and XbaI restriction sites. Polypyrimidine tract binding protein 1 was cloned from HEK293 cDNA, and 3C protease site (LEVLFQGP) was inserted at the N-terminal and inserted into pET28a in between BamHI and HindIII restriction sites, retaining the N-terminal 6X Histidine tag.

EMCV IRES-Luciferase constructs-The firefly luciferase gene was inserted downstream of EMCV IRES in-frame with A-834 residue of IRES to generate the wild-type EMCV IRES-Luciferase construct in pcDNA3.1 (WT-Luc). The CAAAA (RAAA) loop and GCGA (GNRA) loop were mutated to GCTGA and TACG, as per functional assay reports for FMDV IRES and EMCV IRES to generate RAAAmut-Luc and GNRAmut-Luc, respectively (López de Quinto and Martínez-Salas, 1997; Fernández-Miragall and Martínez-Salas, 2003). The sequence of oligos or primers used is listed in Sup. Table 2.

2. Protein overexpression and purification

PTB1 (Histidine tag-3Cprotease site-*PTB1* gene) was overexpressed using 0.5 mM IPTG in *E. coli* BL21 cells at 30 ºC, 120 rpm for 4 hours in Luria broth. 2 l harvested culture was lysed using Buffer N1 (20 mM HEPES pH-7.4, 300 mM KCl, 2 mM $MgCl_2$, 10 % glycerol, 10 mM imidazole, 5 mM β-mercaptoethanol, 0.05 % Triton-X-100, 2 mM PMSF) and sonicated at 18% amplitude, 10 s ON and 20 s OFF pulses, 30 cycles and centrifuges at 20000 rpm for 20 minutes and the supernatant was loaded on Ni-NTA column and eluted using a gradient of N1 to N2 buffer (20 mM HEPES pH-7.4, 300 mM KCl, 2 mM $MgCl_2$, 10 % glycerol, 500 mM imidazole, 5 mM β-mercaptoethanol). PTB1 was eluted at 250 mM Imidazole concentration. The eluant fractions (diluted to 100 mM KCl) were further loaded on Heparin column and eluted by applying a gradient of 100 mM to 1000 mM KCl. The protein was eluted at 250 mM KCl concentration. The eluant fractions were stored at -80 ºC after Size Exclusion Chromatography in Buffer S (20 mM HEPES pH-7.4, 200 mM KCl, 2 mM $MgCl_2$, 5 % glycerol, 1 mM DTT) at 2.5 mg/ml.

3C protease was overexpressed using 0.5 mM IPTG in *E. coli* BL21 cells at 30 ºC, 120 rpm in Luria broth. 2 l harvested culture was lysed using Buffer N11 (20 mM HEPES pH-7.4, 200 mM KCl, 2 mM $MgCl_2$, 10 % glycerol, 10 mM imidazole, 5 mM β-mercaptoethanol, 0.05 % Triton-X-100, 2 mM PMSF) and sonicated at 18 % amplitude, 10 s ON and 20 s OFF pulses, 30 cycles and centrifuges at 20000 rpm for 20 minutes and the supernatant was loaded on Ni-NTA column and eluted using a gradient of N11 to N22 buffer (20 mM HEPES pH-7.4, 200 mM KCl, 2 mM $MgCl_2$, 10 % glycerol, 500 mM imidazole, 5 mM β-mercaptoethanol). 3C protease was eluted at 250 mM imidazole

concentration. The eluant fractions were subjected to Size Exclusion Chromatography in Buffer S (20 mM HEPES pH-7.4, 100 mM KOAc, 2 mM $MgCl_2$, 10% glycerol, 1 mM DTT), and peak fractions were concentrated and stored at 2.5 mg/ml.

3. *In vitro* transcription of EMCV IRES

EMCV IRES 905-pcDNA3.1 was linearized using Xba1 restriction enzyme and transcribed using Promega-RiboMAX™ Large Scale RNA Production Systems as per manufacturer's protocol. 1 µg of linearized plasmid yielded 87 µg of RNA after DNase treatment and RNA cleanup (RNA clean up kit-NEB). WT-Luc, GNRAmut-Luc, and RAAAmut-Luc were linearized using XhoI and transcribed *in vitro* using the same strategy.

4. Assembly of EMCV IRES 48S PIC using Talon Affinity Chromatography

12 µg of IRES was heated at 95 ºC to dissolve any secondary structures acquired and refolded using buffer R (20 mM HEPES pH-7.4, 150 mM KOAc, 2 mM $MgCl_2$, 2 mM β-mercaptoethanol, 0.25 mM spermidine) at 37 ºC for 5 minutes, and PTB1 (1:2 = IRES: PTB1) was added and further incubated at 30ºC for 5 minutes. Simultaneously, Rabbit Reticulocyte Lysate (RRL) (Promega) was incubated at 30ºC with ATP, Amino acid mix minus Leucine, murine RNase Inhibitor for 5 minutes, and then mixed with the IRES-PTB1 vial with instant addition of 6 mM GMP-PnP per reaction (100 µl) and incubated at 30 ºC for 8 minutes, followed by ice incubation. The reaction was loaded onto Talon beads equilibrated with Buffer A (20 mM HEPES, pH 7.4, 150 mM KOAc, 2 mM MgCl2, 4% glycerol, 5 mM imidazole, 2 mM β-mercaptoethanol). After recommended passes, reloading and incubation, the flow through was collected and the beads were washed with Buffer A until A260 attains a baseline value (~0), following which 3C protease in Buffer A was added to the beads and left for overnight incubation. Fractions were eluted using Buffer A (400 µl each in 10 vials) and subjected to analysis such as A260 measurements and agarose gel electrophoresis. Samples having the RNA bands were pelleted using a 1ml sucrose cushion (20 mM HEPES pH-7.4, 150 mM KOAc, 2mM $MgCl_2$, 30% Sucrose, 1mM DTT) in SW60 tubes and centrifuged at 50,000 rpm for 10 hours at 4 ºC. The pellet was resuspended in 20 µl buffer R and used for Cryo-EM grid preparation (no crosslinker was used to avoid artifacts).

5. Negative stain analysis and Mass Spectrometry

The final sample was diluted 10 times using buffer R and applied on 400-mesh Cu TEM grids, which were freshly glow-discharged (negative polarity) for 30 s in GloQube glow-discharge system, stained using 1% Uranyl acetate solution, and analysed using Talos L120C transmission electron microscope at 57000 X magnification. Furthermore, the sample was digested by trypsin and subjected to NanoOrbitrap analysis for the identification of proteins in the complex.

6. Cryo-EM sample preparation

3 µl of resuspended pellet (2.96 A260) was applied on glow-discharged Quantifoil R 1.2/1.3 300 mesh 2nm Carbon Coated Grid and Blotted using 8s and 8.5s Blot time, zero Blot force at 16ºC and 100% Humidity, and plunged into liquid ethane. Cryo-EM data were collected on Talos Arctica transmission electron microscope equipped with a FEG at 200 kV (Thermo Fisher Scientific). All data were collected using a Gatan K2 Summit Direct Detector at a nominal magnification of 36,000 X, and a pixel size of 1.17 Å with a total electron dose of 55 e-/Å2 fractionated over 20 frame movies with a dose rate of ~2.5 e-/$Å^2$ /frame.

6. Data Processing

Micrographs were collected and processed using CryoSPARC v3.3 (Punjani et al 2017). The micrographs were patch motion corrected and CTF was estimated. Using a blob picker with an average diameter of 300 Å particles were picked and extracted. The extracted particles were subjected to multiple rounds of 2D classification. Final 2D classes showing promising ribosome 2D features were selected for *ab initio* reconstruction. The junk was discarded, and the 237054 good

particles were classified into 2 classes using a mask around $tRNA_i$. We obtained 2 classes-Empty 40S (1.25L particles-Class 1 or Map A), and 40S with tRNA bound (1.11L particles-Class 2). Class 2 was further classified into 2 classes using a 3D mask around the IRES density and subjected to non-uniform refinement with global CTF refinement to yield Map B, having $tRNA_i$ and IRES density (55k particles). This was subjected to Non-uniform Refinement (Punjani et al 2020) with global CTF refinement. Map B class was further classified using a mask around eIF2α and eIF2γ to yield 2 classes-40S-$tRNA_i$-IRES-eIF2 (28k particles-Map B1) and 40S-$tRNA_i$-IRES (26k particles). The obtained maps were then subjected to model building and refinement. The local resolution for the obtained maps were estimated using Phenix (Liebschner et al 2019).

7. Map analysis and Model building

To the obtained maps, 40S ribosome (PDB Id-6YAN) was fitted using UCSF Chimera. The 40S head (Head proteins + 18S rRNA (1197-1688) + eS17) and 40S body (Body proteins + 18S rRNA (1-1196; 1689-1870)) was fitted to the obtained maps separately and subjected to Rigid Body Fit and Real Space Refinement using PHENIX (Liebschner et al 2019). The models were merged using Coot (Emsley et al 2010) and subjected to Real Space Refinement. $tRNA_i$ and mRNA models were taken from PDB Id-8OZ0 and fitted to the maps-B and B1 in Chimera. eIF2α and eIF2γ from PDB Id-8OZ0 were rigid-body fitted to Map B1 and then mutated as per Rabbit eIF2 protein sequence (NCBI Reference Sequence-XP_002719561.1; XP_051683593.1) and subjected to a final Real Space Refinement. The IRES I domain apex model was predicted from Alphafold3 (Abramson et al 2024) and the helical sub-domains were dismantled and fitted according to best fit using Chimera, followed by chain joining in Coot with manual Real Space Refinement (Afonine et al 2018). The geometry was corrected using Geometry minimization tool in Phenix with rounds of Real Space Refinement. H domain model was predicted using Alphafold3. The final model yielded 40S-EMCV IRES-$tRNA_i$ (Map B) and 40S-EMCV IRES-$tRNA_i$-eIF2αY (Map B1). All the figures were made using ChimeraX (Pettersen et al 2021). The models were real space refined using Phenix, and the Fourier Shell Correlation for 'Map to Model' for each was determined at 0.5 FSC (Sup. Fig. 2A-C; Table 1).

8. Luciferase assay

WT-Luc, GNRAmut-Luc, and RAAAmut-Luc RNA was subjected to polyadenylation using *E. coli* Poly(A) Polymerase and ATP supplied in New England Biolabs kit using manufacturer's protocol. Post polyadenylation, the RNA was extracted using RNA cleanup kit (NEB). The RNA was denatured at 95 ºC and refolded using buffer R at 37 ºC for 5 minutes. To 1 µg of RNA, 10 µl RRL was added with 0.25 µM amino acid mix minus leucine, and amino acid mix minus methionine, 1 mM ATP, 0.5 mM GTP, and the remaining volume was adjusted using buffer R to a final volume of 30 µl. Each reaction was divided into 3 sets-10 µl each and incubated at 30 ºC for 3 hours. The luciferase activity in each reaction was measured by adding 10 µl of Steady-Glo Luciferase reagent (Promega) and quantified using a Tecan plate reader. The graphs were plotted using Graphpad prism.

9. Secondary Structure Determination and Multiple Sequence Alignments

The secondary structure for I domain apex was obtained from RNAfold (Gruber et al 2008). Multiple sequence alignments were performed using Clustal Omega (Sievers et al 2021). Sequence accession number for various sequence used-EMCV (NC_001479.1), FMDV (NC_039210.1), TMEV (DQ401688.1), TRV (AB090161.1), VHEV (M80888.1), SAFV (FM207487.1), Poliovirus (NC_002058.3).

Table 1. Cryo-EM data and model statistics

Data collection	**Map A- 40S without factors**	**Map B- 40S-tRNA$_i$-EMCV IRES**	**Map B1- 40S-tRNA$_i$-EMCV IRES-eIF2α-eIF2γ**
Microscope	Talos Arctica		
Camera	Gatan K2 Summit Direct Detector		
Magnification	36000X		
Voltage (kV)	200		
Electron dose (e^-/Å^2)	50-55		
Defocus range	-2 to -0.5		
Pixel size (Å)	1.17		
Number of micrographs	22549		
Cryo-EM reconstruction			
Final number of particles	125503	55231	28439
Point group symmetry	C1	C1	C1
Fsc threshold	0.143	0.143	0.143
Map overall resolution (Å)	4.51	4.55	5.01
Resolution metric	Gold-Standard FSC	Gold-Standard FSC	Gold-Standard FSC
Sharpening B factor(Å^2)	-153.5	-117.9	-122.3
Atomic model refinement			
Resolution (0.5) (Å)	5.0	5.4	6.0
D FSC model (0/0.143/0.5)	4.4/4.5/5.0	4.4/4.5/5.4	4.9/4.9/6.0
Initial models used	6YAN	6YAN; 8OZ0	6YAN; 8OZ0
CC overall			
CC(mask)/(box)/(peaks)/(volume)	0.73/0.83/0.72/0.66	0.77/0.84/0.71/0.77	0.78/0.84/0.72/0.78
Molprobity score	2.3	2.28	2.23
Clash score	19.08	19.09	18.64
No. of atoms/ No. of residues			
Chains	39	41	39
Total atoms (Hydrogens:0)	76455	80057	83717
No. of residues-Proteins/Nucleotides	4916/1744	4918/1912	5660/1912
Bond (RMSD) Lengths (Å)	0.002	0.003	0.003
Bond (RMSD) Angles (^{o})	0.658	0.650	0.659
Ramachandran plot (%)			
Outliers	0.21	0.27	0.20
Allowed	8.94	8.21	7.09
Favored	90.86	91.52	92.72
Rotamer outliers (%)	0.02	0.02	0.00
Cβ outliers (%)	0.00	0.00	0.00
CaBLAM outliers (%)	6.09	5.82	5.47

Data availability

Maps and atomic coordinates of the 40S ribosome (Map A), 40S ribosome-EMCV IRES-tRNAi (Map B) and 40S ribosome-EMCV IRES-ternary complex (Map B1) have been deposited in the EMDB database with accession codes- EMD-64646, EMD-64644, and EMD-64645, respectively and in the PDB database with accession code- 9UZM, 9UZK, and 9UZL, respectively.

Acknowledgements

EMCV IRES (nt 280–905) into pCR2.1 was a kind gift from Dr. Bruno Sargueil, CNRS UMR8015, Universit'e Paris Descartes, France and 3C protease-pET24 was a kind gift from Prof. Raghavan Varadarajan, Indian Institute of Science (IISc), India. We thank various central facilities, namely Cryo-EM, Mass Spectrometry and Computational cluster at the Division of Biological Sciences, IISc for support. DD acknowledges the DBT-JRF Programme for fellowship. The authors acknowledge the DST-FIST support to the department. This work was supported by the Intermediate Fellowship from DBT-Welcome Trust India Alliance to TH (IA/I/17/2/503313).

Additional files

Supplementary Figures and Tables

Supplementary movie 1. The movie depicts the position of EMCV IRES (brown) on the 40S ribosomal subunit, in contact with tRNAi (green) in a 48S PIC state. On zooming, the IRES- domain I apical part is contacting the ribosomal proteins- uS13 (golden yellow) and uS19 (violet); elbow and acceptor arm of tRNAi which is base-paired to start codon.

Additional information

Funding

Funder	Grant reference number	Author
Wellcome Trust DBT India Alliance (India Alliance)	IA/I/17/2/503313	Tanweer Hussain

Author ORCID iDs

Deepakash Das: https://orcid.org/0009-0000-3138-4033
Tanweer Hussain: https://orcid.org/0000-0003-4735-2380

References

Abaeva IS, Young C, Warsaba R, Khan N, Tran LV, Jan E, Pestova TV, Hellen CUT (2023) The structure and mechanism of action of a distinct class of dicistrovirus intergenic region IRESs. *Nucleic Acids Res* **51**:9294-9313 https://doi.org/10.1093/nar/gkad569 | PubMed | PubMed Central

Abdullah SW, Wu J, Wang X, Guo H, Sun S (2023) Advances and Breakthroughs in IRES-Directed Translation and Replication of Picornaviruses. *mBio* **14**:e0035823 https://doi.org/10.1128/mbio.00358-23 | PubMed | PubMed Central

Abramson J, Adler J, Dunger J, Evans R, Green T, Pritzel A, Ronneberger O, Willmore L, Ballard AJ, Bambrick J, *et al.* (2024) Accurate structure prediction of biomolecular interactions with AlphaFold 3. *Nature* **630**:493-500 https://doi.org/10.1038/s41586-024-07487-w | PubMed | PubMed Central

Acosta-Reyes F, Neupane R, Frank J, Fernández IS (2019) The Israeli acute paralysis virus IRES captures host ribosomes by mimicking a ribosomal state with hybrid tRNAs. *EMBO J* **38**:e102226 https://doi.org/10.15252/embj.2019102226 | PubMed | PubMed Central

Afonine PV, Poon BK, Read RJ, Sobolev OV, Terwilliger TC, Urzhumtsev A, Adams PD (2018) Real-space refinement in PHENIX for cryo-EM and crystallography. *Acta Crystallogr D Struct Biol* **74**:531-544 https://doi.org/10.1107/S2059798318006551 | PubMed | PubMed Central

Baglioni C, Simili M, Shafritz DA (1978) Initiation activity of EMC virus RNA, binding to initiation factor eIF-4B and shut-off of host cell protein synthesis. *Nature* **275**:240-3 https://doi.org/10.1038/275240a0 | PubMed

Ban N, Beckmann R, Cate JH, Dinman JD, Dragon F, Ellis SR, Lafontaine DL, Lindahl L, Liljas A, Lipton JM, *et al.* (2014) A new system for naming ribosomal proteins. *Curr Opin Struct Biol* **24**:165-9 https://doi.org/10.1016/j.sbi.2014.01.002 | PubMed | PubMed Central

Ben-Shem A, de Loubresse N Garreau, Melnikov S, Jenner L, Yusupova G, Yusupov M (2011) The structure of the eukaryotic ribosome at 3.0 Å resolution. *Science* **334**:1524-9 https://doi.org/10.1126/science.1212642 | PubMed

Bhattacharjee S, Abaeva IS, Brown ZP, Arhab Y, Fallah H, Hellen CUT, Frank J, Pestova TV (2025) The mechanism of ribosomal recruitment during translation initiation on Type 2 IRESs. *bioRxiv* https://doi.org/10.1101/2025.06.11.659010 | PubMed | PubMed Central

Boehringer D, Thermann R, Ostareck-Lederer A, Lewis JD, Stark H (2005) Structure of the hepatitis C virus IRES bound to the human 80S ribosome: remodeling of the HCV IRES. *Structure* **13**:1695-706 https://doi.org/10.1016/j.str.2005.08.008 | PubMed

Bowen AM, Musalgaonkar S, Moomau CA, Gulay SP, Mirvis M, Dinman JD (2015) Ribosomal protein uS19 mutants reveal its role in coordinating ribosome structure and function. *Translation* **3**:e1117703 https://doi.org/10.1080/21690731.2015.1117703 | PubMed | PubMed Central

Brito Querido J, Díaz-López I, Ramakrishnan V (2024) The molecular basis of translation initiation and its regulation in eukaryotes. *Nat Rev Mol Cell Biol* **25**:168-186 https://doi.org/10.1038/s41580-023-00624-9 | PubMed

Brito Querido J, Sokabe M, Díaz-López I, Gordiyenko Y, Fraser CS, Ramakrishnan V (2024) The structure of a human translation initiation complex reveals two independent roles for the helicase eIF4A. *Nat Struct Mol Biol* **31**:455-464 https://doi.org/10.1038/s41594-023-01196-0 | PubMed | PubMed Central

Brito Querido J, Sokabe M, Kraatz S, Gordiyenko Y, Skehel JM, Fraser CS, Ramakrishnan V (2020) Structure of a human 48*S* translational initiation complex. *Science* **369**:1220-1227 https://doi.org/10.1126/science.aba4904 | PubMed | PubMed Central

Brown ZP, Abaeva IS, De S, Hellen CUT, Pestova TV, Frank J (2022) Molecular architecture of 40S translation initiation complexes on the hepatitis C virus IRES. *EMBO J* **41**:e110581 https://doi.org/10.15252/embj.2022110581 | PubMed | PubMed Central

Carocci M, Bakkali-Kassimi L (2012) The encephalomyocarditis virus. *Virulence* **3**:351-67 https://doi.org/10.4161/viru.20573 | PubMed | PubMed Central

Chamond N, Deforges J, Ulryck N, Sargueil B (2014) 40S recruitment in the absence of eIF4G/4A by EMCV IRES refines the model for translation initiation on the archetype of Type II IRESs. *Nucleic Acids Res* **42**:10373-84 https://doi.org/10.1093/nar/gku720 | PubMed | PubMed Central

Datey A, Sharma P, Khaja FT, Rahil H, Hussain T (2025) Yeast Eukaryotic Initiation Factor 4B Remodels the MRNA Entry Site on the Small Ribosomal Subunit. *Biochemistry* **64**:600-608 https://doi.org/10.1021/acs.biochem.4c00489 | PubMed

de Breyne S, Yu Y, Unbehaun A, Pestova TV, Hellen CU (2009) Direct functional interaction of initiation factor eIF4G with type 1 internal ribosomal entry sites. *Proc Natl Acad Sci U S A* **106**:9197-202 https://doi.org/10.1073/pnas.0900153106 | PubMed | PubMed Central

des Georges A, Dhote V, Kuhn L, Hellen CU, Pestova TV, Frank J, Hashem Y (2015) Structure of mammalian eIF3 in the context of the 43S preinitiation complex. *Nature* **525**:491-5 https://doi.org/10.1038/nature14891 | PubMed | PubMed Central

Dorn G, Gmeiner C, de Vries T, Dedic E, Novakovic M, Damberger FF, Maris C, Finol E, Sarnowski CP, Kohlbrecher J, *et al.* (2023) Integrative solution structure of PTBP1-IRES complex reveals strong compaction and ordering with residual conformational flexibility. *Nat Commun* **14**:6429 https://doi.org/10.1038/s41467-023-42012-z | PubMed | PubMed Central

Duke GM, Hoffman MA, Palmenberg AC (1992) Sequence and structural elements that contribute to efficient encephalomyocarditis virus RNA translation. *J Virol* **66**:1602-9 https://doi.org/10.1128/JVI.66.3.1602-1609.1992 | PubMed | PubMed Central

Eliseev B, Yeramala L, Leitner A, Karuppasamy M, Raimondeau E, Huard K, Alkalaeva E, Aebersold R, Schaffitzel C (2018) Structure of a human cap-dependent 48S translation pre-initiation complex. *Nucleic Acids Res* **46**:2678-2689 https://doi.org/10.1093/nar/gky054 | PubMed | PubMed Central

Emsley P, Lohkamp B, Scott WG, Cowtan K (2010) Features and development of Coot. *Acta Crystallogr D Biol Crystallogr* **66**:486-501 https://doi.org/10.1107/S0907444910007493 | PubMed | PubMed Central

Fernández IS, Bai XC, Murshudov G, Scheres SH, Ramakrishnan V (2014) Initiation of translation by cricket paralysis virus IRES requires its translocation in the ribosome. *Cell* **157**:823-31 https://doi.org/10.1016/j.cell.2014.04.015 | PubMed | PubMed Central

Fernández N, Fernandez-Miragall O, Ramajo J, García-Sacristán A, Bellora N, Eyras E, Briones C, Martínez-Salas E (2011) Structural basis for the biological relevance of the invariant apical stem in IRES-mediated translation. *Nucleic Acids Res* **39**:8572-85 https://doi.org/10.1093/nar/gkr560 | PubMed | PubMed Central

Fernández-Miragall O, de Quinto S López, Martínez-Salas E (2009) Relevance of RNA structure for the activity of picornavirus IRES elements. *Virus Res* **139**:172-82 https://doi.org/10.1016/j.virusres.2008.07.009 | PubMed

Fernández-Miragall O, Martínez-Salas E (2003) Structural organization of a viral IRES depends on the integrity of the GNRA motif. *RNA* **9**:1333-44 https://doi.org/10.1261/rna.5950603 | PubMed | PubMed Central

Fiore JL, Nesbitt DJ (2013) An RNA folding motif: GNRA tetraloop-receptor interactions. *Q Rev Biophys* **46**:223-64 https://doi.org/10.1017/S0033583513000048 | PubMed

Gruber AR, Lorenz R, Bernhart SH, Neuböck R, Hofacker IL (2008) The Vienna RNA websuite. *Nucleic Acids Res* **36**:W70-W74 https://doi.org/10.1093/nar/gkn188 | PubMed | PubMed Central

Hashem Y, des Georges A, Dhote V, Langlois R, Liao HY, Grassucci RA, Pestova TV, Hellen CU, Frank J (2013) Hepatitis-C-virus-like internal ribosome entry sites displace eIF3 to gain access to the 40S subunit. *Nature* **503**:539-43 https://doi.org/10.1038/nature12658 | PubMed | PubMed Central

Hashem Y, des Georges A, Dhote V, Langlois R, Liao HY, Grassucci RA, Hellen CU, Pestova TV, Frank J (2013) Structure of the mammalian ribosomal 43S preinitiation complex bound to the scanning factor DHX29. *Cell* **153**:1108-19 https://doi.org/10.1016/j.cell.2013.04.036 | PubMed | PubMed Central

Hellen CU, Wimmer E (1995) Translation of encephalomyocarditis virus RNA by internal ribosomal entry. *Curr Top Microbiol Immunol* **203**:31-63 https://doi.org/10.1007/978-3-642-79663-0_2 | PubMed

Hinnebusch AG (2017) Structural Insights into the Mechanism of Scanning and Start Codon Recognition in Eukaryotic Translation Initiation. *Trends Biochem Sci* **42**:589-611 https://doi.org/10.1016/j.tibs.2017.03.004 | PubMed

Hussain T, Llácer JL, Fernández IS, Munoz A, Martin-Marcos P, Savva CG, Lorsch JR, Hinnebusch AG, Ramakrishnan V (2014) Structural changes enable start codon recognition by the eukaryotic translation initiation complex. *Cell* **159**:597-607 https://doi.org/10.1016/j.cell.2014.10.001 | PubMed | PubMed Central

Imai S, Kumar P, Hellen CU, D'Souza VM, Wagner G (2016) An accurately preorganized IRES RNA structure enables eIF4G capture for initiation of viral translation. *Nat Struct Mol Biol* **23**:859-64 https://doi.org/10.1038/nsmb.3280 | PubMed | PubMed Central

Imai S, Suzuki H, Fujiyoshi Y, Shimada I (2023) Dynamically regulated two-site interaction of viral RNA to capture host translation initiation factor. *Nat Commun* **14**:4977 https://doi.org/10.1038/s41467-023-40582-6 | PubMed | PubMed Central

International Committee on Taxonomy of Viruses Executive Committee (2020) The new scope of virus taxonomy: partitioning the virosphere into 15 hierarchical ranks. *Nat Microbiol* **5**:668-674 https://doi.org/10.1038/s41564-020-0709-x | PubMed | PubMed Central

Jackson RJ, Hellen CU, Pestova TV (2010) The mechanism of eukaryotic translation initiation and principles of its regulation. *Nat Rev Mol Cell Biol* **11**:113-27 https://doi.org/10.1038/nrm2838 | PubMed | PubMed Central

Jang SK, Kräusslich HG, Nicklin MJ, Duke GM, Palmenberg AC, Wimmer E (1988) A segment of the 5' nontranslated region of encephalomyocarditis virus RNA directs internal entry of ribosomes during in vitro translation. *J Virol* **62**:2636-43 https://doi.org/10.1128/JVI.62.8.2636-2643.1988 | PubMed | PubMed Central

Johnson AG, Grosely R, Petrov AN, Puglisi JD (2017) Dynamics of IRES-mediated translation. *Philos Trans R Soc Lond B Biol Sci* **372**:20160177 https://doi.org/10.1098/rstb.2016.0177 | PubMed | PubMed Central

Kafasla P, Morgner N, Pöyry TA, Curry S, Robinson CV, Jackson RJ (2009) Polypyrimidine tract binding protein stabilizes the encephalomyocarditis virus IRES structure via binding multiple sites in a unique orientation. *Mol Cell* **34**:556-68 https://doi.org/10.1016/j.molcel.2009.04.015 | PubMed

Kafasla P, Morgner N, Robinson CV, Jackson RJ (2010) Polypyrimidine tract-binding protein stimulates the poliovirus IRES by modulating eIF4G binding. *EMBO J* **29**:3710-22 https://doi.org/10.1038/emboj.2010.231 | PubMed | PubMed Central

Kaminski A, Belsham GJ, Jackson RJ (1994) Translation of encephalomyocarditis virus RNA: parameters influencing the selection of the internal initiation site. *EMBO J* **13**:1673-81 https://doi.org/10.1002/j.1460-2075.1994.tb06431.x | PubMed | PubMed Central

Khatter H, Myasnikov AG, Natchiar SK, Klaholz BP (2015) Structure of the human 80S ribosome. *Nature* **520**:640-5 https://doi.org/10.1038/nature14427 | PubMed

Kim H, Kim K, Kwon T, Kim DW, Kim SS, Kim YJ (2015) Secondary structure conservation of the stem-loop IV sub-domain of internal ribosomal entry sites in human rhinovirus clinical isolates. *Int J Infect Dis* **41**:21-8 https://doi.org/10.1016/j.ijid.2015.10.015 | PubMed

Kolupaeva VG, Pestova TV, Hellen CU, Shatsky IN (1998) Translation eukaryotic initiation factor 4G recognizes a specific structural element within the internal ribosome entry site of encephalomyocarditis virus RNA. *J Biol Chem* **273**:18599-604 https://doi.org/10.1074/jbc.273.29.18599 | PubMed

Kozak M (1989) The scanning model for translation: an update. *J Cell Biol* **108**:229-41 https://doi.org/10.1083/jcb.108.2.229 | PubMed | PubMed Central

Kwon OS, An S, Kim E, Yu J, Hong KY, Lee JS, Jang SK (2017) An mRNA-specific tRNAi carrier eIF2A plays a pivotal role in cell proliferation under stress conditions: stress-resistant translation of c-Src mRNA is mediated by eIF2A. *Nucleic Acids Res* **45**:296-310 https://doi.org/10.1093/nar/gkw1117 | PubMed | PubMed Central

Lee KM, Chen CJ, Shih SR (2017) Regulation Mechanisms of Viral IRES-Driven Translation. *Trends Microbiol* **25**:546-561 https://doi.org/10.1016/j.tim.2017.01.010 | PubMed

Liang Z, Kumar AS, Jones MS, Knowles NJ, Lipton HL (2008) Phylogenetic analysis of the species Theilovirus: emerging murine and human pathogens. *J Virol* **82**:11545-54 https://doi.org/10.1128/JVI.01160-08 | PubMed | PubMed Central

Liebschner D, Afonine PV, Baker ML, Bunkóczi G, Chen VB, Croll TI, Hintze B, Hung LW, Jain S, McCoy AJ, *et al.* (2019) Macromolecular structure determination using X-rays, neutrons and electrons: recent developments in Phenix. *Acta Crystallogr D Struct Biol* **75**:861-877 https://doi.org/10.1107/S2059798319011471 | PubMed | PubMed Central

Llácer JL, Hussain T, Marler L, Aitken CE, Thakur A, Lorsch JR, Hinnebusch AG, Ramakrishnan V (2015) Conformational Differences between Open and Closed States of the Eukaryotic Translation Initiation Complex. *Mol Cell* **59**:399-412 https://doi.org/10.1016/j.molcel.2015.06.033 | PubMed | PubMed Central

Llácer JL, Hussain T, Dong J, Villamayor L, Gordiyenko Y, Hinnebusch AG (2021) Large-scale movement of eIF3 domains during translation initiation modulate start codon selection. *Nucleic Acids Res* **49**:11491-11511 https://doi.org/10.1093/nar/gkab908 | PubMed | PubMed Central

Lomakin IB, Hellen CU, Pestova TV (2000) Physical association of eukaryotic initiation factor 4G (eIF4G) with eIF4A strongly enhances binding of eIF4G to the internal ribosomal entry site of encephalomyocarditis virus and is required for internal initiation of translation. *Mol Cell Biol* **20**:6019-29 https://doi.org/10.1128/mcb.20.16.6019-6029.2000 | PubMed | PubMed Central

López de Quinto S, Martínez-Salas E (1997) Conserved structural motifs located in distal loops of aphthovirus internal ribosome entry site domain 3 are required for internal initiation of translation. *J Virol* **71**:4171-5 https://doi.org/10.1128/JVI.71.5.4171-4175.1997 | PubMed | PubMed Central

Lozano G, Martínez-Salas E (2015) Structural insights into viral IRES-dependent translation mechanisms. *Curr Opin Virol* **12**:113-20 https://doi.org/10.1016/j.coviro.2015.04.008 | PubMed

Lozano G, Francisco-Velilla R, Martinez-Salas E (2018) Ribosome-dependent conformational flexibility changes and RNA dynamics of IRES domains revealed by differential SHAPE. *Sci Rep* **8**:5545 https://doi.org/10.1038/s41598-018-23845-x | PubMed | PubMed Central

Maloney A, Joseph S (2024) Validating the EMCV IRES Secondary Structure with Structure-Function Analysis. *Biochemistry* **63**:107-115 https://doi.org/10.1021/acs.biochem.3c00579 | PubMed | PubMed Central

Maris C, Jayne S, Damberger FF, Beusch I, Dorn G, Ravindranathan S, Allain FH (2020) A transient α-helix in the N-terminal RNA recognition motif of polypyrimidine tract binding protein senses RNA secondary structure. *Nucleic Acids Res* **48**:4521-4537 https://doi.org/10.1093/nar/gkaa155 | PubMed | PubMed Central

Martinez-Salas E, Francisco-Velilla R, Fernandez-Chamorro J, Embarek AM (2018) Insights into Structural and Mechanistic Features of Viral IRES Elements. *Front Microbiol* **8**:2629 https://doi.org/10.3389/fmicb.2017.02629 | PubMed | PubMed Central

Martínez-Salas E, Francisco-Velilla R, Fernandez-Chamorro J, Lozano G, Diaz-Toledano R (2015) Picornavirus IRES elements: RNA structure and host protein interactions. *Virus Res* **206**:62-73 https://doi.org/10.1016/j.virusres.2015.01.012 | PubMed

Muhs M, Hilal T, Mielke T, Skabkin MA, Sanbonmatsu KY, Pestova TV, Spahn CM (2015) Cryo-EM of ribosomal 80S complexes with termination factors reveals the translocated cricket paralysis virus IRES. *Mol Cell* **57**:422-32 https://doi.org/10.1016/j.molcel.2014.12.016 | PubMed | PubMed Central

Murray J, Savva CG, Shin BS, Dever TE, Ramakrishnan V, Fernández IS (2016) Structural characterization of ribosome recruitment and translocation by type IV IRES. *eLife* **5**:e13567 https://doi.org/10.7554/eLife.13567 | PubMed | PubMed Central

Neupane R, Pisareva VP, Rodriguez CF, Pisarev AV, Fernández IS (2020) A complex IRES at the 5'-UTR of a viral mRNA assembles a functional 48S complex via an uAUG intermediate. *eLife* **9**:e54575 https://doi.org/10.7554/eLife.54575 | PubMed | PubMed Central

Niepmann M, Gerresheim GK (2020) Hepatitis C Virus Translation Regulation. *Int J Mol Sci* **21**:2328 https://doi.org/10.3390/ijms21072328 | PubMed | PubMed Central

Ochs K, Saleh L, Bassili G, Sonntag VH, Zeller A, Niepmann M (2002) Interaction of translation initiation factor eIF4B with the poliovirus internal ribosome entry site. *J Virol* **76**:2113-22 https://doi.org/10.1128/jvi.76.5.2113-2122.2002 | PubMed | PubMed Central

Pelletier J, Sonenberg N (1988) Internal initiation of translation of eukaryotic mRNA directed by a sequence derived from poliovirus RNA. *Nature* **334**:320-5 https://doi.org/10.1038/334320a0 | PubMed

Pestova TV, Hellen CU, Shatsky IN (1996) Canonical eukaryotic initiation factors determine initiation of translation by internal ribosomal entry. *Mol Cell Biol* **16**:6859-69 https://doi.org/10.1128/MCB.16.12.6859 | PubMed | PubMed Central

Petrov A, Grosely R, Chen J, O'Leary SE, Puglisi JD (2016) Multiple Parallel Pathways of Translation Initiation on the CrPV IRES. *Mol Cell* **62**:92-103 https://doi.org/10.1016/j.molcel.2016.03.020 | PubMed | PubMed Central

Petrychenko V, Yi SH, Liedtke D, Peng BZ, Rodnina MV, Fischer N (2024) Structural basis for translational control by the human 48S initiation complex. *Nat Struct Mol Biol* https://doi.org/10.1038/s41594-024-01378-4 | PubMed

Pettersen EF, Goddard TD, Huang CC, Couch GS, Greenblatt DM, Meng EC, Ferrin TE (2004) UCSF Chimera--a visualization system for exploratory research and analysis. *J Comput Chem* **25**:1605-12 https://doi.org/10.1002/jcc.20084 | PubMed

Pettersen EF, Goddard TD, Huang CC, Meng EC, Couch GS, Croll TI, Morris JH, Ferrin TE (2021) UCSF ChimeraX: Structure visualization for researchers, educators, and developers. *Protein Sci* **30**:70-82 https://doi.org/10.1002/pro.3943 | PubMed | PubMed Central

Punjani A, Rubinstein JL, Fleet DJ, Brubaker MA (2017) cryoSPARC: algorithms for rapid unsupervised cryo-EM structure determination. *Nat Methods* **14**:290-296 https://doi.org/10.1038/nmeth.4169 | PubMed

Punjani A, Zhang H, Fleet DJ (2020) Non-uniform refinement: adaptive regularization improves single-particle cryo-EM reconstruction. *Nat Methods* **17**:1214-1221 https://doi.org/10.1038/s41592-020-00990-8 | PubMed

Quade N, Boehringer D, Leibundgut M, van den Heuvel J, Ban N (2015) Cryo-EM structure of Hepatitis C virus IRES bound to the human ribosome at 3.9-Å resolution. *Nat Commun* **6**:7646 https://doi.org/10.1038/ncomms8646 | PubMed | PubMed Central

Reiter NJ, Osterman A, Torres-Larios A, Swinger KK, Pan T, Mondragón A (2010) Structure of a bacterial ribonuclease P holoenzyme in complex with tRNA. *Nature* **468**:784-9 https://doi.org/10.1038/nature09516 | PubMed | PubMed Central

Roberts LO, Belsham GJ (1997) Complementation of defective picornavirus internal ribosome entry site (IRES) elements by the coexpression of fragments of the IRES. *Virology* **227**:53-62 https://doi.org/10.1006/viro.1996.8312 | PubMed

Robertson ME, Seamons RA, Belsham GJ (1999) A selection system for functional internal ribosome entry site (IRES) elements: analysis of the requirement for a conserved GNRA tetraloop in the encephalomyocarditis virus IRES. *RNA* **5**:1167-79 https://doi.org/10.1017/s1355838299990301 | PubMed | PubMed Central

Scheper GC, Thomas AA, Voorma HO (1991) The 5' untranslated region of encephalomyocarditis virus contains a sequence for very efficient binding of eukaryotic initiation factor eIF-2/2B. *Biochim Biophys Acta* **1089**:220-6 https://doi.org/10.1016/0167-4781(91)90011-a | PubMed

Scheper GC, Voorma HO, Thomas AA (1994) Binding of eukaryotic initiation factor-2 and trans-acting factors to the 5' untranslated region of encephalomyocarditis virus RNA. *Biochimie* **76**:801-9 https://doi.org/10.1016/0300-9084(94)90084-1 | PubMed

Sievers F, Higgins DG (2021) The Clustal Omega Multiple Alignment Package. *Methods Mol Biol* **2231**:3-16 https://doi.org/10.1007/978-1-0716-1036-7_1 | PubMed

Simonetti A, Guca E, Bochler A, Kuhn L, Hashem Y (2020) Structural Insights into the Mammalian Late-Stage Initiation Complexes. *Cell Rep* **31**:107497 https://doi.org/10.1016/j.celrep.2020.03.061 | PubMed | PubMed Central

Spahn CM, Jan E, Mulder A, Grassucci RA, Sarnow P, Frank J (2004) Cryo-EM visualization of a viral internal ribosome entry site bound to human ribosomes: the IRES functions as an RNA-based translation factor. *Cell* **118**:465-75 https://doi.org/10.1016/j.cell.2004.08.001 | PubMed

Spahn CM, Kieft JS, Grassucci RA, Penczek PA, Zhou K, Doudna JA, Frank J (2001) Hepatitis C virus IRES RNA-induced changes in the conformation of the 40s ribosomal subunit. *Science* **291**:1959-62 https://doi.org/10.1126/science.1058409 | PubMed

Sweeney TR, Abaeva IS, Pestova TV, Hellen CU (2014) The mechanism of translation initiation on Type 1 picornavirus IRESs. *EMBO J* **33**:76-92 https://doi.org/10.1002/embj.201386124 | PubMed | PubMed Central

Trono D, Pelletier J, Sonenberg N, Baltimore D (1988) Translation in mammalian cells of a gene linked to the poliovirus 5' noncoding region. *Science* **241**:445-8 https://doi.org/10.1126/science.2839901 | PubMed

Velazquez MA, Nuthalapati SS, Hankinson J, Fominykh K, Lulla V, Sweeney TR, Hill CH (2025) Structural and mechanistic insights into translation initiation on the enterovirus Type 1 IRES. *bioRxiv* https://doi.org/10.1101/2025.10.04.680434

Villa N, Do A, Hershey JW, Fraser CS (2013) Human eukaryotic initiation factor 4G (eIF4G) protein binds to eIF3c, -d, and -e to promote mRNA recruitment to the ribosome. *J Biol Chem* **288**:32932-40 https://doi.org/10.1074/jbc.M113.517011 | PubMed | PubMed Central

Villamayor-Belinchón L, Sharma P, Gordiyenko Y, Llácer JL, Hussain T (2024) Structural basis of AUC codon discrimination during translation initiation in yeast. *Nucleic Acids Res* **52**:11317-11335 https://doi.org/10.1093/nar/gkae737 | PubMed | PubMed Central

Welnowska E, Sanz MA, Redondo N, Carrasco L (2011) Translation of viral mRNA without active eIF2: the case of picornaviruses. *PLoS One* **6**:e22230 https://doi.org/10.1371/journal.pone.0022230 | PubMed | PubMed Central

Yamamoto H, Collier M, Loerke J, Ismer J, Schmidt A, Hilal T, Sprink T, Yamamoto K, Mielke T, Bürger J, *et al.* (2015) Molecular architecture of the ribosome-bound Hepatitis C Virus internal ribosomal entry site RNA. *EMBO J* **34**:3042-58 https://doi.org/10.15252/embj.201592469 | PubMed | PubMed Central

Yamamoto H, Unbehaun A, Loerke J, Behrmann E, Collier M, Bürger J, Mielke T, Spahn CM (2014) Structure of the mammalian 80S initiation complex with initiation factor 5B on HCV-IRES RNA. *Nat Struct Mol Biol* **21**:721-7 https://doi.org/10.1038/nsmb.2859 | PubMed

Yi SH, Petrychenko V, Schliep JE, Goyal A, Linden A, Chari A, Urlaub H, Stark H, Rodnina MV, Adio S, *et al.* (2022) Conformational rearrangements upon start codon recognition in human 48S translation initiation complex. *Nucleic Acids Res* **50**:5282-5298 https://doi.org/10.1093/nar/gkac283 | PubMed | PubMed Central

Yokoyama T, Machida K, Iwasaki W, Shigeta T, Nishimoto M, Takahashi M, Sakamoto A, Yonemochi M, Harada Y, Shigematsu H, *et al.* (2019) HCV IRES Captures an Actively Translating 80S Ribosome. *Mol Cell* **74**:1205-1214.e8. https://doi.org/10.1016/j.molcel.2019.04.022 | PubMed

Yu Y, Abaeva IS, Marintchev A, Pestova TV, Hellen CU (2011) Common conformational changes induced in type 2 picornavirus IRESs by cognate trans-acting factors. *Nucleic Acids Res* **39**:4851-65 https://doi.org/10.1093/nar/gkr045 | PubMed | PubMed Central

Zhao J, Li Y, Wang C, Zhang H, Zhang H, Jiang B, Guo X, Song X (2020) IRESbase: A Comprehensive Database of Experimentally Validated Internal Ribosome Entry Sites. *Genomics Proteomics Bioinformatics* **18**:129-139 https://doi.org/10.1016/j.gpb.2020.03.001 | PubMed | PubMed Central

Peer reviews

Reviewer #1 (Public review):

Summary:

The authors have studied how a virus (EMCV) uses its RNA (Type 2 IRES) to hijack the host's protein-making machinery. They use cryo-EM to extract structural information about the recruitment of viral Type 2 IRES to ribosomal pre-IC. The authors propose a novel interaction

mechanism in which the EMCV Type 2 IRES mimics 28S rRNA and interacts with ribosomal proteins and initiator tRNA (tRNAi).

Strengths:

(1) Getting structural insights about the Type 2 IRES-based initiation is novel.

(2) The study allows a good comparison of other IRES-based initiation systems.

(3) The manuscript is well-written and clearly explains the background, methods, and results.

Comments on revised version:

I have gone through the revised manuscript by Das and Hussain along with the rebuttal comments. While the poor resolution of the ribosomal complex limits detailed analysis of the molecular interactions, addition of the luciferase reporter assay in the supplementary has enriched the paper.

https://doi.org/10.7554/eLife.107788.2.sa3

Reviewer #2 (Public review):

Summary:

The field of protein translation has long sought the structure of a Type 2 Internal Ribosome Entry Site (IRES). In this work, Das and Hussain pair cryo-EM with algorithmic RNA structure prediction to present a structure of the Type 2 IRES found in Encephalomyocarditis virus (EMCV). Using medium to low resolution cryo-EM maps, they resolve the overall shape of a critical domain of this Type 2 IRES. They use algorithmic RNA prediction to model this domain onto their maps and attempt to explain previous results using this model.

Strengths:

(1) This study reveals a previously unknown/unseen binding modality used by IRESes: a direct interaction of the IRES with the initiator tRNA.

(2) Use of an IRES-associated factor to assemble and pull down an IRES bound to the small subunit of the ribosome from cellular extracts is innovative.

(3) Algorithmic modeling of RNA structure to complement medium to low resolution cryo-EM maps, as employed here, can be implemented for other RNA structures.

Comments on revised version:

Thanks to the authors for providing thorough responses to the reviewer questions and comments. I appreciate their attempts of improving overall resolution of the complex via various processing strategies that the reviewers suggested.

The authors interpretations of their cryo-EM data match those reported by Bhattacharjee et al. 2025 (EMCV-IRES 48S) and can be contextualized in the light of Velazquez et al. 2025 (poliovirus IRES-48S).

The authors' contextualization of their results with previously published studies (Discussion section lines 355-402) is satisfactory to me but can be improved.

https://doi.org/10.7554/eLife.107788.2.sa2

Reviewer #3 (Public review):

Summary:

Type II IRES, such as those from encephalomyocarditis virus (EMCV) and foot-and-mouth disease virus (FMDV), mediate cap-independent translation initiation by using the full complement of eukaryotic initiation factors (eIFs), except the cap-binding protein eIF4E. The molecular details of how IRES type II interacts with the ribosome and initiation factors to promote recruitment have remained unclear. Das and Hussain used cryo-electron microscopy to determine the structure of a translation initiation complex assembled on the EMCV IRES. The structure reveals a direct interaction between the IRES and the 40S ribosomal subunit, offering mechanistic insight into how type II IRES elements recruit the ribosome.

Strengths:

The structure reveals a direct interaction between the IRES and the 40S ribosomal subunit, offering mechanistic insight into how type II IRES elements recruit the ribosome.

Comments on revised version:

The revised manuscript does not improve the resolution; however, the authors provide a detailed and well-reasoned rationale that directly addresses the concerns I raised about their structural interpretation. In addition, two independent preprints have been released since the initial submission. In one case, the authors report a higher-resolution, and importantly, all three studies present consistent assignments and interpretations. Together, these observations strengthen confidence in the authors' conclusions. I therefore do not have major concerns regarding the publication of this revised manuscript.

https://doi.org/10.7554/eLife.107788.2.sa1

Author response:

The following is the authors' response to the original reviews.

> ***eLife Assessment***
>
> *This manuscript offers valuable structural and mechanistic insights into the structure and assembly of the Type II internal ribosome entry site (IRES) from encephalomyocarditis virus (EMCV) and the translation initiation complex, revealing a direct interaction between the IRES and the 40S ribosomal subunit. While a solid cryo-EM method was used, enhancing the overall resolution or adding complementary biochemical data would further improve the clarity and impact of this study. This manuscript will attract researchers in cap-independent translation, host-pathogen interactions, and virology.*

We thank the editorial team for a favourable assessment and for mentioning our work as 'valuable'. In the following sections, we have addressed the weaknesses and recommendations pointed out by the Reviewers and hope for an improvement in the description of this work.

> ***Public Reviews:***
>
> ***Reviewer #1 (Public review):***
>
> *Summary:*

> *The authors have studied how a virus (EMCV) uses its RNA (Type 2 IRES) to hijack the host's protein-making machinery. They use cryo-EM to extract structural information about the recruitment of viral Type 2 IRES to ribosomal pre-IC. The authors propose a novel interaction mechanism in which the EMCV Type 2 IRES mimics 28S rRNA and interacts with ribosomal proteins and initiator tRNA (tRNAi).*
>
> *Strengths:*
>
> *(1) Getting structural insights about the Type 2 IRES-based initiation is novel.*
>
> *(2) The study allows a good comparison of other IRES-based initiation systems.*
>
> *(3) The manuscript is well-written and clearly explains the background, methods, and results.*

We thank Reviewer 1 for appreciating our efforts and finding structural insights about the Type 2 IRES-based initiation presented in this study as novel.

> *Weaknesses:*
>
> *(1) The main weakness of the work is the low resolution of the structure. This limits the possibility of data interpretation at the molecular level.*
>
> *However, despite the moderate resolution of the cryo-EM reconstructions, the model fits well into the density. The analysis of the EMCV IRES-48S PIC structure is thorough and includes meaningful comparisons to previously published structures (e.g., PDB IDs - 7QP6 and 7QP7). These comparisons showed that Map B1 represents a closed conformation, in contrast to Map A in the open state (Figure 2). Additionally, the proposed 28S rRNA mimicry strategy supported by structural superposition with the 80S ribosome and sequence similarity between the I domain of the IRES and the h38 region of 28S rRNA (Fig. 4) is well-justified.*

We agree that the low resolution of the map has compromised the data interpretation at the molecular level, and we thank the reviewer for appreciating our findings at this resolution. Due to the low resolution, we have reported findings for stretches or regions such as the domain I loops and stems, rather than individual nucleotides.

> *(2) The lack of experimental validation of the functional importance of regions like the GNRA and RAAA loops is another limitation of this study.*

We agree about the lack of additional experiments other than Cryo-EM for probing the importance of regions such as GNRA and RAAA loops in this study. Previously, multiple studies have reported on the importance of GNRA and RAAA loops and we have cited them in the manuscript. The essentiality of RAAA loop for type 2 IRES was demonstrated in earlier report López de Quinto and Martínez-Salas, 1997 (Cited in manuscript). Further, the conservation of this loop across the type 2 IRES family adds to the importance of this loop (Manuscript Figure 6B). This loop and its flanking G-C stem are similar to h38 of 28S rRNA, and it appears that RAAA loop adopts a mimicry mechanism to interact with the 40S ribosomal protein- uS19, thus highlighting its importance for interaction with 40S. Experiments destabilising the G-C stem also compromise IRES activity, as shown for the case of FMDV IRES (Fernández et al 2011). Previous studies related to the mutation of the GNRA or GCGA loop in EMCV IRES have shown a deficiency in IRES activity (Roberts and Belsham, 1997; Robertson et al 1999), suggesting the importance of these regions in the viral IRES biology, and these reports are cited in the manuscript. Not only EMCV IRES, but mutation in the GUAA (representative of GNRA) loop of FMDV IRES also showed a significant reduction in IRES activity (López de Quinto and Martínez-Salas, 1997). In this work, we observe that the GCGA loop interacts with $tRNA_i$ in the EMCV IRES-48S PIC, thus implicating the importance of

this loop. Moreover, incubation of FMDV IRES with 40S ribosomes has shown a decrease in SHAPE reactivity in domain 3 apex (position 170- 200 nucleotides) (Lozano et al 2018), which corresponds to EMCV IRES domain I apex.

However, to address this concern in the revised manuscript we mutated these loops and performed luciferase assay (Supplementary figure 4 A). The results showed decreased IRES activity (Pg 10) and correlated with previous reports demonstrating the importance of these regions for overall IRES activity.

> *(3) Minor modifications related to data processing and biochemical studies will further validate and strengthen the findings.*
>
> *(a) In the cryo-EM data section, the authors should include an image showing rejected particles during 2D classification. This would help readers understand why, despite having over 22k micrographs with sufficient particle distribution and good contrast, only a smaller number of particles were used in the final reconstruction. Additionally, employing map-sharpening tools such as Ewald sphere correction, Bayesian polishing, or reference-based motion correction might further improve the quality of the maps. Targeting high-resolution structures would be particularly informative.*

We have included the image for rejected 2D classes (Author response image 1). We agree with the Reviewer's query related to the huge number of micrographs and relatively smaller number of particles for the final reconstruction. Since the total number of micrographs (22000) is the summation of multiple datasets, prepared and collected at different times, the distribution of the particles per micrograph was not uniform in all sessions, ranging from good to poor. Among these, around 8000 micrographs have poor particle number and distribution. As a result, the number of particles per micrograph is heterogeneous across the compiled dataset, and only 237054 ribosomal particles were obtained after multiple rounds of 2D and 3D classification. Further, the final reconstruction was performed using particles obtained after masked classification for IRES and ternary complex density. Only the particles that show the best density for both IRES and ternary complex are used for this map. Another set of particles that have only a portion of IRES and NO density for ternary complex forms another map. And we have a third map with an empty 40S.

We thank the reviewer for the suggestions to improve the quality of the maps further. As suggested, we started with the processing of the data. However, during this process the common computational cluster that were using for this data processing had to be physically relocated, and unfortunately after the relocation we faced technical issues in accessing and continuing with the processing. Several attempts to resolve the issue with the help of IT team failed. Thus, we lost 3-4 months without any progress. Therefore, we used Relion on our in-house workstation to process the data files from the start, as our in-house computational resources are unequipped to run cryoSPARC processes (for large dataset due to memory limitations).

We reprocessed the datasets in Relion5 and did 'Bayesian Processing', for reference-based beam-induced motion correction per-particle. Post-processing, we used cryoSPARC to merge the particles and tried classifying the good ribosome particles using focus-based masked classification, as shown in Supplementary Figure 1.1. However, this processing did not improve the resolution, as Map B (containing 40S, tRNA, IRES) had an overall resolution of 4.8 Å (Author response image 2). Therefore, we would like to report the same maps as given in the initial submission.

We estimated the time to redo the entire processing using cryoSPARC on the common computational cluster, and it would take us another 3-4 months or more and we do not anticipate a massive improvement in the extra density.

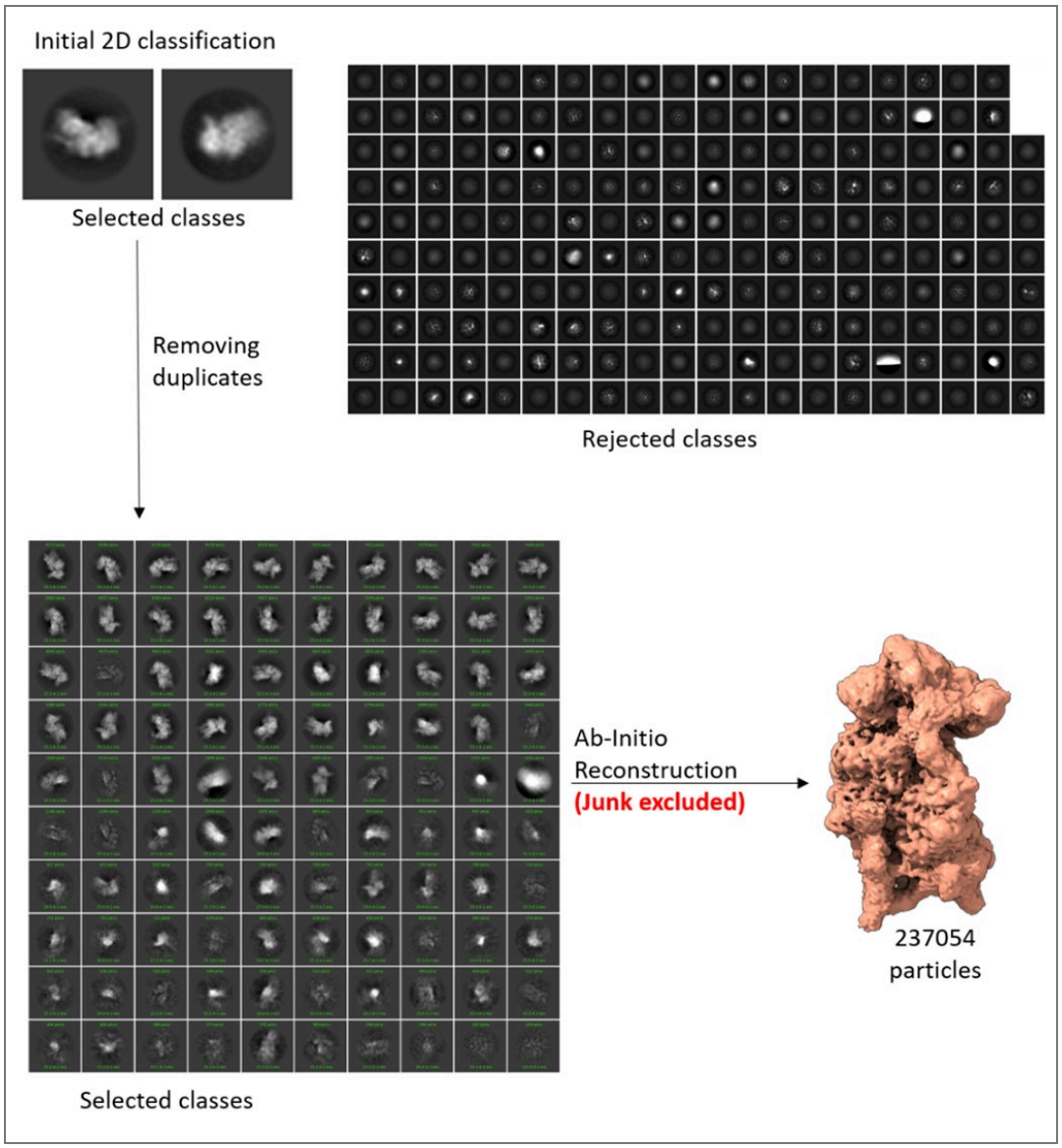

Author response image 1. **The selected 2D classes and the rejected 2D classes from initial round of classification, and the final selected 2D classes, which were subjected to Ab-initio reconstruction to get the good ribosome particles.**

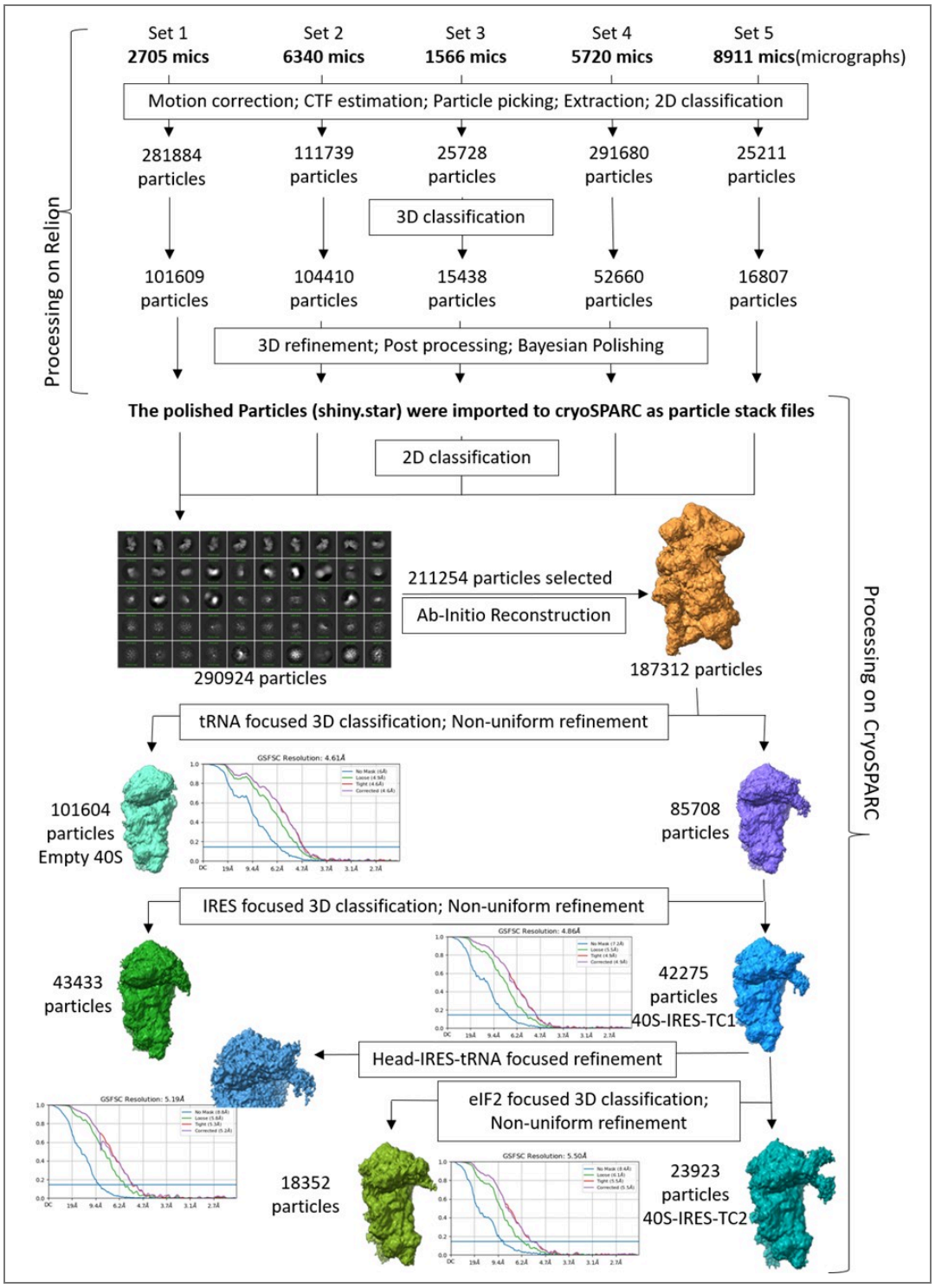

Author response image 2. **Reprocessing of the entire dataset using Relion5 for polishing of selected particles, followed by 3D classification and refinements in cryoSPARC.**

> *(b) The strategic modelling of different IRES domains into the density, particularly the domain into the region above the 40S head, is appreciable. However, providing the full RNA tertiary structure (RNAfold) of the EMCV IRES (nucleotides 280-905) would better explain the logic behind the model building and its molecular interpretation.*

We thank the reviewer for appreciating the modelling of the domain I apex in the cryo-EM density. We tried to predict the full tertiary structure of the IRES using Alphafold3; however,

inclusion of the full-length sequence from 280-905 gave models of extremely low confidence (Author response image 3), and a few domains do not abide by the secondary structure of EMCV IRES as reported in Duke et al 1992.

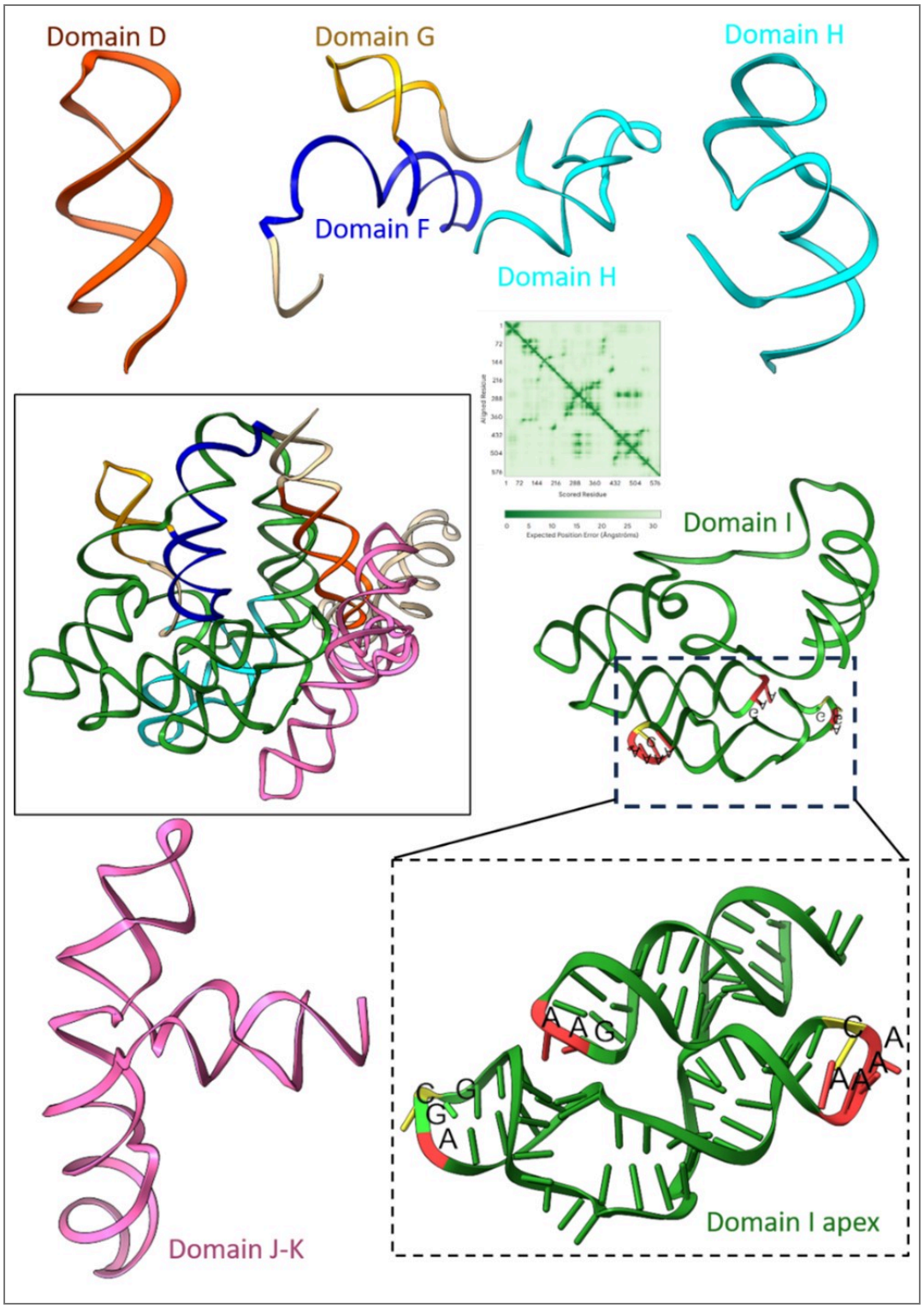

Author response image 3. Prediction of tertiary structure of EMCV IRES (280-905 nucleotides) and zoomed features for each domain present in the IRES. The predicted aligned error plot for the RNA structure is shown.

We used individual domains of EMCV IRES and predicted the tertiary structure, independent of other IRES domain using Alphafold3. As a result, the confidence scores improved, and the

tertiary structures also correlated with the experimentally determined EMCV IRES secondary structure (Duke et al 1992; Maloney and Joseph, 2024). Although the overall tertiary structure of EMCV IRES is lacking, recent studies were able to solve the structures of EMCV IRES domains in complex with their respective binding proteins. We superimposed the independently predicted domains D, E, and F tertiary structure on the NMR ensemble of IRES domain D to F with PTB1 (Dorn et al 2023), where the predicted domains fit in the experimental model. Similarly, we used the cryo-EM structure of domain J-K-eIF4G-eIF4A (Imai et al 2023) and found a close fit with the predicted structures. The analysis highlighted that the domain I apex serves as the best fit with the extra density with respect to architecture and fitting. This analysis is now added in the revised manuscript in Supplementary figure- 3.2.

Furthermore, 3D structural models of FMDV IRES domains 2, 3, and 4 (corresponding to EMCV IRES domains- H, I, and J-K) were predicted from SHAPE reactivity values and RNAComposer server (Figure 3, Lozano et al 2018). The predicted architecture of domain 3 apex (FMDV IRES) coincides with our domain I apex model (EMCV IRES).

> *(c) Although the authors compare their findings with other types of IRESs (Types 1, 3, and 4), there is no experimental validation of the functional importance of regions like the GNRA and RAAA loops. Including luciferase-based assays or mutational studies of these regions for validation of structural interpretations is strongly recommended.*

We have discussed the possibility of how the other IRESs, such as type 1 and type 5, might use similar strategies as EMCV IRES to assemble the 48S PIC, given the similarity in the motif sequence and position across the viral IRESs. Like EMCV IRES, the type 1 IRES (Poliovirus, Coxsackie virus, etc.) also harbours the GNRA loop, preceded by a C-rich loop at its longest domain, known for long-range RNA-RNA interactions. The segment harbouring GNRA loop is highly conserved across the type 1 family of IRESs (Kim et al 2015). The Aichi viral IRES harbours a GNRA loop in its longest domain, that is, domain J. Deletion of the GNRA loop has compromised the IRES activity; however, substitution mutations in this region have elevated the IRES activity or remained unaltered (Yu et al 2011). We have hypothesized that these IRESs might use the GNRA motifs in their longest domain (domain IV in type 1, and domain J in Aichi virus- type 5) based on the location and architecture to that of EMCV IRES, where GNRA is present in the longest domain (I) and preceded by a C-rich loop where it can potentially mediate long-range interactions with $tRNA_i$, as all these IRESs require eIF2-ternary complex for the formation of 48S PIC. Parallelly, like EMCV IRES, type 1 and type 5 IRESs have the placement of this GNRA motif-containing domain before the eIF4G-binding domain. Thus, we suggest the possibility of adoption of a similar strategy by these IRESs to interact with $tRNA_i$ during the formation of 48S PIC. During the revision of this work a preprint reported the structure of polioviral IRES-48S PIC where domain IV apex (similar to domain I apex in EMCV IRES) interacts with uS13 and uS19, and the GNRA loop directly interacts with $tRNA_i$ during start codon recognition (Velazquez et al 2025). We hypothesize that Aichiviral IRES might use this motif to mediate long-range interactions with $tRNA_i$, similar to type 1 and type 2 IRESs, as all these IRESs require eIF2-ternary complex for the formation of 48S PIC.

> ***Reviewer #2 (Public review):***
>
> *Summary:*
>
> *The field of protein translation has long sought the structure of a Type 2 Internal Ribosome Entry Site (IRES). In this work, Das and Hussain pair cryo-EM with algorithmic RNA structure prediction to present a structure of the Type 2 IRES found in Encephalomyocarditis virus (EMCV). Using medium to low resolution cryo-EM maps, they resolve the overall shape of a critical domain of this Type 2 IRES. They use algorithmic RNA prediction to model this domain onto their maps and attempt to explain previous results using this model.*

> *Strengths:*
>
> *(1) This study reveals a previously unknown/unseen binding modality used by IRESes: a direct interaction of the IRES with the initiator tRNA.*
>
> *(2) Use of an IRES-associated factor to assemble and pull down an IRES bound to the small subunit of the ribosome from cellular extracts is innovative.*
>
> *(3) Algorithmic modeling of RNA structure to complement medium to low resolution cryo-EM maps, as employed here, can be implemented for other RNA structures.*

We thank Reviewer 2 for positive and encouraging comments on our work, appreciating our 'innovative' approach of using IRES-associated factor to assemble and pull down the IRES-bound ribosomal complex.

> *Weaknesses:*
>
> *(1) Maps at the resolution presented prevent unambiguous modelling of the EMCV-IRES. This, combined with the lack of any biochemical data, calls into question any inferences made at the level of individual nucleotides, such as the GNRA loop and CAAA loop (Figure 4).*

We understand the concerns raised by the reviewer related to the resolution of the EMCV IRES-48S PIC map. We refrained from commenting on individual nucleotides or molecular interactions in the manuscript. Instead, we discuss loops, RNA stretches or motifs that could be inferred with more confidence in the IRES density as shown in Figure 4. The EMCV IRES can directly interact with the 40S ribosome using its domain H and I (Chamond et al 2014), however, the details of this interaction were unknown. We observe that the CAAA loop of domain I apex interacts with 40S ribosome based on the placement of a portion of domain I in the cryo-EM map. This is also reflected in the SHAPE data (Chamond et al 2014- Supplementary figures 2, and 8), where a decrease in reactivity is evident in the presence of 40S ribosome. In addition, incubation of EMCV IRES with rabbit reticulocyte lysate (RRL) offered protection to domain I apex regions, which included the CAAA loop (Maloney and Joseph, 2024- Figure 4b).

Furthermore, this decrease in SHAPE reactivity pattern is evident for FMDV IRES domain 3 apex (similar to domain I in EMCV IRES) in the presence of 40S ribosome (Lozano et al 2018). Thus, these studies are consistent with the placement of IRES model in the cryo-EM map. Moreover, we performed structural analysis (mentioned above) which showed that the domain I apex serves as the best fit with the extra density with respect to architecture and fitting (Supplementary figure- 3.2).

> *(2) The EMCV IRES contains an upstream AUG at position 826, where the PIC can assemble (Pestova et al 1996; PMID 8943341). It is unclear if this start codon was mutated in this study. If it were not mutated, placement of AUG-834 over AUG-826 in the P-site is unexplained.*

We thank the reviewer for bringing up this point, as we missed mentioning this in the initial submission. The EMCV IRES does not require scanning and directly positions the AUG-834 at the P site (Pestova et al 1996). In Pestova et al 1996, the intensity of the toeprint at AUG-834 is more intense than that of AUG-826. Further, AUG-834 lies in the Kozak context, whereas AUG-826 has a poor Kozak context, and AUG-826 codon is not in-frame with AUG-834. Therefore, the synthesis of the polypeptide requires AUG-834 at the P site. In our cryo-EM map, we observed that the $tRNA_i$ is in a P_{IN} state, which indicates the recognition of the start codon, and we reasoned that it is more likely that AUG-834 is placed at the P site than AUG-826. We have mentioned this in the revised manuscript as we had NOT mutated AUG-826 (Pg 8).

> *(3) The claims the authors make about (i) the general overall shape and binding site of the IRES, (ii) its gross interaction with the two ribosomal proteins, (iii) the P-in state of the*

> *48S, (iv) the rearrangement of the ternary complex are all warranted. Their claims about individual nucleotides or smaller stretches of the IRES-without any supporting biochemical data-is not warranted by the data.*

We thank the reviewer for warranting major claims, and due to the low-resolution we have reported findings for stretches or regions such as the domain I loops and stems, rather than individual nucleotides. The interaction of domain I apical region with uS13, uS19, and $tRNA_i$ is also observed the high-resolution structure of reconstituted EMCV IRES-48S PIC that was reported in a preprint while our work was under peer review process (Bhattacharjee et al 2025). Thus, the reconstituted EMCV IRES-48S PIC (Bhattacharjee et al 2025) also supports our assignment of domain I and its conserved loops, interacting with ribosome and $tRNA_i$.

> ***Reviewer #3 (Public review):***
>
> *Summary:*
>
> *Type II IRES, such as those from encephalomyocarditis virus (EMCV) and foot-and-mouth disease virus (FMDV), mediate cap-independent translation initiation by using the full complement of eukaryotic initiation factors (eIFs), except the cap-binding protein eIF4E. The molecular details of how IRES type II interacts with the ribosome and initiation factors to promote recruitment have remained unclear. Das and Hussain used cryo-electron microscopy to determine the structure of a translation initiation complex assembled on the EMCV IRES. The structure reveals a direct interaction between the IRES and the 40S ribosomal subunit, offering mechanistic insight into how type II IRES elements recruit the ribosome.*
>
> *Strengths:*
>
> *The structure reveals a direct interaction between the IRES and the 40S ribosomal subunit, offering mechanistic insight into how type II IRES elements recruit the ribosome.*
>
> *Weaknesses:*
>
> *While this reviewer acknowledges the technical challenges inherent in determining the structure of such a highly flexible complex, the overall resolution remains insufficient to fully support the authors' conclusions, particularly given that cryo-EM is the sole experimental approach presented in the manuscript.*
>
> *The study is biologically significant; however, the authors should improve the resolution or include complementary biochemical validation.*

We thank Reviewer 3 for acknowledging the technical challenges in this study and finding our study biologically significant. We understand the concerns related to low resolution and the requirement of complementary biochemical validation for our reported observations and interpretations in the manuscript. We tried to improve the resolution, but the improvement was not sufficient to resolve the IRES at the nucleotide level. Independently, another group has reported the same findings at a higher resolution while our work was under peer review process (Bhattacharjee et al 2025), which corroborates our structural data on EMCV IRES and its interaction with ribosome and $tRNA_i$ in its 48S PIC stage. Further, in the revised manuscript we also present biochemical validation for GNRA and RAAA loops in EMCV IRES. We mutated these loops and performed luciferase assay (Supplementary figure 4 A). The results showed decreased IRES activity (Pg 10) and correlated with previous reports (Roberts and Belsham, 1997; López de Quinto and Martínez-Salas, 1997; Robertson et al 1999) demonstrating the importance of these regions for overall IRES activity.

> ***Reviewing Editor Comments:***
>
> *The reviewers' comments are appended. While the reviewers acknowledge the complexity associated with this system, they also raised concerns about the modeling of RNA and*

registering its sequence in low-resolution maps. We believe that the strength of evidence and overall impact of your study can be elevated by providing higher-resolution cryo-EM data or complementary biochemical studies and addressing reviewers' concerns.

Reviewer #2 (Recommendations for the authors):

(1) Science:

Have the authors tried a focused refinement (local refinement in cryoSPARC) using a generous mask that encloses the head and the IRES but excludes the ternary complex and the body of the 40S? This can be done with all the particles in map B (~55K) and has the possibility of improving the resolution of domain I which can be subsequently used to build a better model of the IRES. See the middle right panel, light yellow colored mask in Figure 1A in PMID 37659578 for the type of mask being suggested.

We did another round of 2D classification to eliminate any residual junk in the ~55k particle set, corresponding to Map B. Post classification, 49439 particles were selected and refined using non-uniform refinement to get Map B11. The overall resolution of Map B11 was 4.6 Å. Thereafter, we made a mask around the 40S head-IRES-tRNA on Map B11 and subjected the class for local refinement. The overall local resolution in the masked region improved to 4.5 Å (Author response image 4).

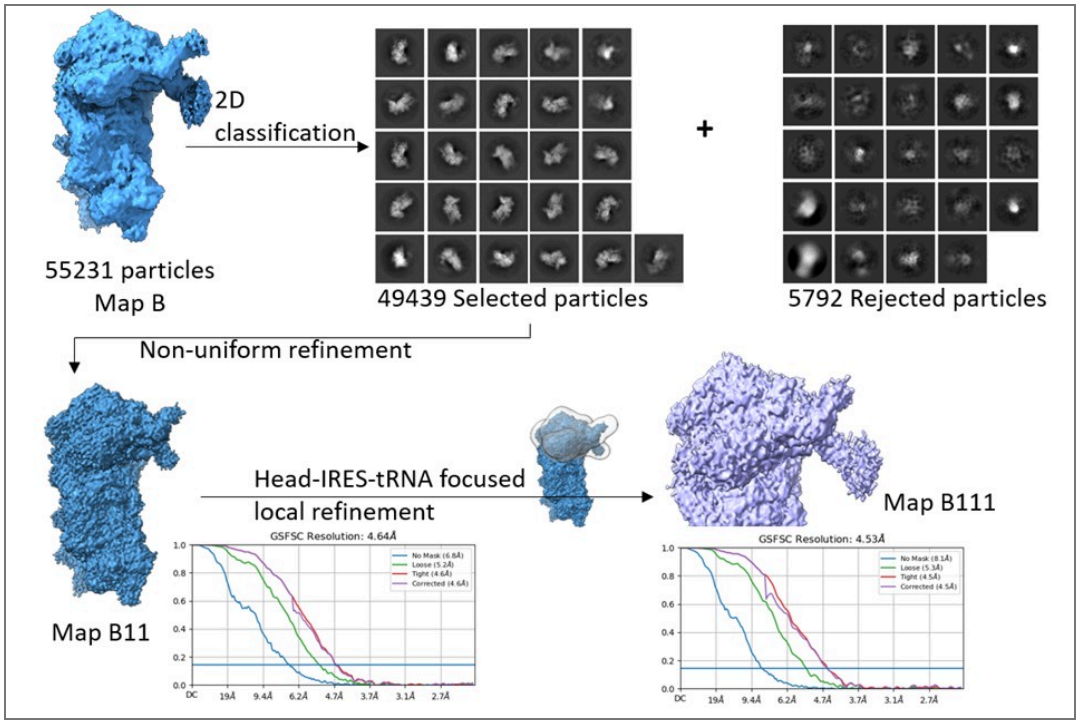

Author response image 4. Data processing- Map B particles were 2D classified, and further junk was cleared as rejected particles. The selected particles were refined using non-uniform refinement to get Map B11, and later, a focused mask circling the head-tRNA-IRES region was used for local refinement in the region to yield map B111.

We estimated the local resolution across the focused region in Map B111 and compared this with that of Map B (Author response image 5). The local refinement shows minor improvement in the local resolution in this region, and is not sufficient to resolve the IRES density at the level of nucleotides.

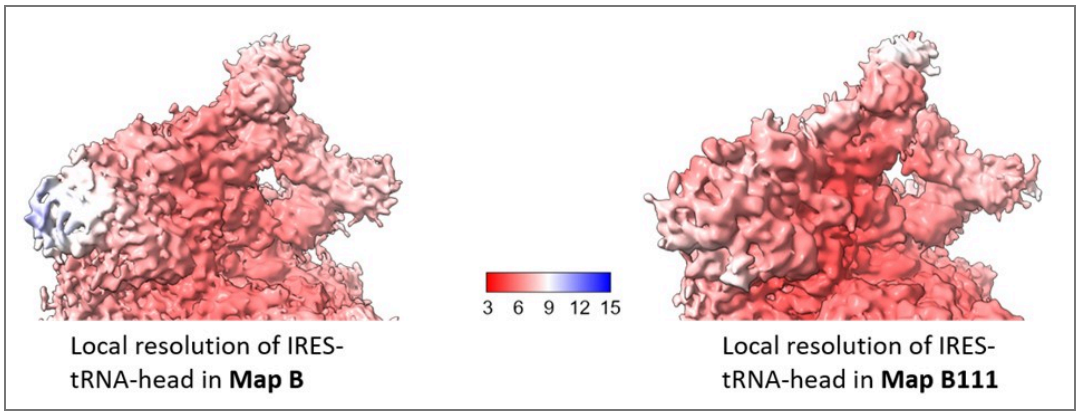

Author response image 5. **Comparison of local resolution across head-IRES-tRNA in map B1 (as reported in the manuscript) and Map B111.**

> *(2) Presentation:*
>
> *(a) Please use the previously established convention of naming the domains: "domain I", "domain H", etc, instead of "I domain" or "J-K domain" while describing parts of the IRES.*

We have made the changes as per the established convention.

> *(b) Figure 2B reports a 6.9 A distance vs. 7 A in the text. Please use ~ or approximately to keep numbers consistent.*

We have used ~ symbol to suggest the approximate distance.

> *(c) References missing on page 15 when referring to "previously determined HCV and CrPV structures".*

We have added the references (Pg 12).

> *(d) Please edit the text for typos and sentence structure.*

The typos and sentence structure were corrected wherever necessary.

> *(e) Some phrases and sentences (e.g. last few sentences of the first paragraph in the discussion) could be rewritten for clarity.*

Previous sentence- “The domain I of EMCV IRES is similar to domain IV of polioviral IRES (or other type 1 IRESs such as Coxsackie viral IRES) in terms of length, secondary structure, and conserved motifs (GNRA, C-rich) positioning (Fig. 6C), therefore, anticipating a similar interaction with $tRNA_i$, highlighting a sequestering tendency by competing with cellular mRNAs.”

Rephrased sentence- “Like EMCV IRES, the type 1 IRES (Poliovirus, Coxsackie virus, etc.) also harbours the GNRA loop, preceded by a C-rich loop at its longest domain, known for long-range RNA-RNA interactions. The segment harbouring GNRA loop is highly conserved across the type 1 family of IRESs (Kim et al 2015). The domain I of EMCV IRES is similar to domain IV of polioviral IRES or other type 1 IRESs in terms of length, secondary structure, and conserved motifs (GNRA, C-rich) positioning (Fig. 6C). Therefore, we anticipate a similar interaction of domain IV (in type 1 IRES class) with $tRNA_i$. Also, this interaction of IRES with $tRNA_i$ could be a strategy by which these IRESs can sequester the $tRNA_i$ pool in the cell, rendering them unavailable for capped cellular mRNAs.”

> ***Reviewer #3 (Recommendations for the authors):***
>
> *(1) For the revision process, the authors provided three atomic models alongside their corresponding cryo-EM density maps, including a 48S complex in closed conformation. Given this conformation, it is reasonable to interpret the structure as representing a post-start codon recognition state (late-stage initiation). However, this reviewer finds that*

> *the local resolution within the mRNA channel is insufficient to support the atomic model building as presented. The density does not allow for an unambiguous assignment of nucleotides in this region; the authors should either improve the local resolution or remove the modeled mRNA from the structure.*

We understand the concern of the Reviewer. Although the mRNA density in the channel is poor, we modelled the mRNA with AUG-834 at the P site because the known biology of EMCV IRES. The EMCV IRES does not require scanning and directly positions the AUG-834 at the P site (Pestova et al 1996). In Pestova et al 1996, the intensity of the toeprint at AUG-834 is more intense than that of AUG-826. Further, AUG-834 lies in the Kozak context, whereas AUG-826 has a poor Kozak context, and AUG-826 codon is not in-frame with AUG-834. Therefore, the synthesis of the polypeptide requires AUG-834 at the P site. In our cryo-EM map, we observed that the $tRNA_i$ is in a P_{IN} state, which indicates the recognition of the start codon, and we reasoned that it is very likely that AUG-834 is placed at the P site.

> *(2) As noted by the authors, the start codon in the EMCV IRES is positioned within a strong Kozak sequence. The nucleotide at position -3 is known to interact with eIF2α, yet, in the current model, A831 is positioned such that physical contact with eIF2α would be structurally impossible. This discrepancy raises concerns about the accuracy of the modeled eIF2α, which, like other regions of the structure, is not clearly supported by the cryo-EM density. The authors should revise the atomic model of eIF2α to ensure it is consistent with the experimental map and established molecular interactions.*

In our analysis of EMCV IRES-48S PIC, we could observe eIF2α and eIF2γ in Map B and B1. However, the local resolution was low to model the entire protein with side-chains (Supplementary figure 1.2 A). So, we used rigid body fitting of eIF2α and eIF2γ (Author response image 6). From the model, we could trace the backbone of Arg55, however could not resolve the side chain. Similarly, the mRNA in the channel was modelled based on placement of AUG-834 at the P site for EMCV IRES, which enabled us to model the flanking residues, rather than at the nucleotide-level resolution. We anticipate that a higher resolution structure will be able to capture this interaction of eIF2α with mRNA nucleotide (-3), therefore refrained from commenting on this interaction in the manuscript. In the revised manuscript, we have removed the side chains of eIF2α and eIF2γ, and kept the Cα-backbone only. The map-model statistics of map B1 is updated in table 1.

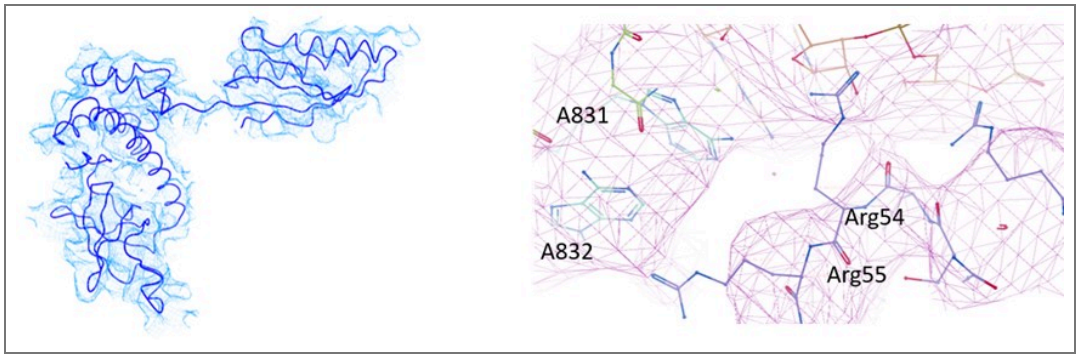

Author response image 6. (left) Fitting of eIF2α model in the map. (right) Fitting of Cα backbone of eIF2α and mRNA in the map.

> *(3) The authors observed additional density interacting with ribosomal proteins uS19 and uS13, and tRNA, which they tentatively assign to domain I of the IRES. Although the local resolution in this region does not allow an unambiguous assignment, the interpretation is reasonable. However, further structural and functional validation is necessary to support this assignment. The authors should improve the local resolution, either by performing focused refinement or by increasing the number of particles used in the reconstruction.*

The assignment of the extra density to domain I of the IRES was based on the architecture of the density. This density allows no other IRES domain to fit in this region (Supplementary figure 3.2). We tried to improve the local resolution using focused refinement, but the resolution was insufficient to resolve the IRES at the nucleotide level. Please see the above-mentioned comments in this regard on Pg 12.

> *(4) Figure 5 shows a slight shift in the position of the ternary complex. Is the observed tRNA conformation compatible with the structural rearrangements required for 60S subunit joining?*

During the transition of 48S PIC to 80S elongation-competent complex, there are major changes in the conformation of $tRNA_i$, due to the joining of eIF5B, and release of eIF2 (Petrychenko et al 2024). This joining event of eIF5B positions the $tRNA_i$ elbow and acceptor stem towards the 40S body to aid 60S ribosomal subunit joining (Petrychenko et al 2024). However, in the context of EMCV IRES-48S PIC, we observed that the position of $tRNA_i$ elbow and acceptor stem is towards the 40S head, and away from the body. On superimposing the human 48S PIC structure (before 60S joining), 48S-5 (PDB Id- 8PJ5- Petrychenko et al 2024), we note that $tRNA_i$ in EMCV IRES-48S PIC is away from the canonical $tRNA_i$ position (in contact with eIF5B). Therefore, we anticipate a change in $tRNA_i$ conformation during eIF5B joining and eIF2 release. This hypothesis coincides with the fact that the IRES interacting with the $tRNA_i$ elbow needs to be displaced from the position to facilitate the interaction of $tRNA_i$ with eIF5B. Moreover, this rearrangement would also aid in 60S joining and prevent any clash with the IRES domain I. We have added this in Results selection 5 and Figure 5D.

> *(5) In the discussion section, the authors state: "eIF3-eIF4G interaction is dispensable for EMCV IRES-48S PIC formation, so we do not rule out the possibility that EMCV IRES may dislodge eIF3 from its position on the solvent surface as observed in the case of HCV IRES (Hashem et al, 2013)." This statement is highly speculative. Is there any experimental or structural evidence to support this proposed mechanism in the context of EMCV IRES?*

Previous biochemical reports on the eIF3-eIF4G interaction suggested that eIF4G residues from 1011-1104 interact with eIF3 (Villa et al 2013). In the context of EMCV IRES, this region of eIF4G is not required to form 48S PIC on the IRES, suggesting the eIF3-eIF4G interaction is dispensable for EMCV IRES-48S PIC formation. However, the recent structure of the human canonical 48S PIC has shown that the eIF4G-HEAT1 domain can interact with eIF3 subunits c, h, and l, and that eIF4G-bound eIF4A can interact with 40S ribosomal protein eS7, thus mediating the interaction between eIF4-bound mRNA and the 43S PIC (Brito Querido et al 2024) but the known eIF3-binding region in eIF4G was not captured in the map. Although the canonical eIF3-eIF4G interaction is essential in the case of cap-dependent initiation, this interaction could be dispensable for 48S PIC formation on EMCV IRES. In case of HCV IRES-mediated initiation, eIF3 is displaced from its canonical position that facilitates the binding of HCV IRES to 40S ribosomal subunit (Hashem et al 2013). We did not see any density corresponding to eIF3 in the obtained maps. Further, we have used focused classification using a mask on the canonical eIF3 position; however, we do not see any density corresponding to eIF3 in the EMCV IRES-48S PIC complex. Therefore, we hypothesized the possibility that eIF3 might be dislodged from its canonical binding site on the 40S ribosomal subunit. However, as per the recent independent report on EMCV IRES-48S PIC, eIF3 is present in the complex (Bhattarcharjee et al 2025).

Hence, we have rephrased the existing sentence- “However, eIF3-eIF4G interaction is dispensable for EMCV IRES-48S PIC formation, so we do not rule out the possibility that EMCV IRES may dislodge eIF3 from its position on the solvent surface as observed in case of HCV IRES (Hashem et al 2013).”

Rephrased sentence- “However, the canonical eIF3-eIF4G interaction (Villa et al 2013) is dispensable for EMCV IRES-48S PIC formation (Lomakin et al 2000; Sweeney et al 2014), and we do not see any density for eIF3 even after focused classification. However, as per the

recent independent report on reconstituted EMCV IRES-48S PIC, eIF3 is present in the complex at the canonical position (Bhattarcharjee et al 2025). This position of eIF3 further highlights the possibility that eIF4G-eIF4A proteins are also placed similarly to the canonical eIF3-eIF4G-eIF4A position (Brito Querido et al 2024) in context to EMCV IRES-48S PIC. Thus, placing eIF4G-domain J-K close to ES6 of 40S ribosome, which coincides with the previous hydroxyl radical cleavage assay (Yu et al 2011)."

> *(6) eIF4A has been shown to directly interact with eIF3 and facilitate recruitment of the 43S PIC. Does the interaction of the J-K domain with eIF4G/eIF4A, compatible with the known eIF4A-eIF3 interaction within the 43S PIC? In other words, during EMCV IRES-mediated initiation, could the eIF4A-eIF3 interaction functionally substitute for the eIF4G-eIF3 interaction?*

Reports on EMCV IRES-mediated translation initiation have shown eIF4G as an essential component of 48S PIC formation (Pestova et al 1996; Lomakin et al 2000; Kolupaeva et al 2003; Sweeney et al 2014), where eIF4G directly interacts with domain J-K of IRES and eIF4A, thus enabling loading of eIF4A on the IRES. In our study, the cryo-EM map of EMCV IRES-48S PIC lacks density for eIF3 and eIF4 proteins, and locating eIF4F is challenging due to the inherent flexibility associated with the complex. Previous studies on EMCV IRES-48S PIC have mapped the location of eIF4G close to ES6 towards the platform side of the body and eIF3 using the hydroxyl radical cleavage assay (Yu et al 2011). The human 48S initiation complex structures have shown a similar location for eIF4G, which is at the mRNA exit site, contacting eIF3 (Brito Querido et al 2020; Brito Querido et al 2024). On overlapping the 18S rRNA of EMCV IRES-48S PIC to that of the human 48S PIC in closed conformation (PDB Id- 8OZ0), and further superimposing the J-K-St- eIF4G- eIF4A (PDB Id- 8HUJ) on human 48S PIC (PDB Id- 8OZ0) with respect to HEAT1 of eIF4G, the domain J-K becomes positioned at the subunit face of 40S body, close to ES6 (Author response image 7). This correlates with the previously reported position for eIF4G with respect to EMCV IRES-48S PIC (Yu et al 2011). The predicted model shows no clashes with the canonical eIF4A-eIF3/ eIF4G-eIF4A-eIF3 interaction, or with the domain J-K-eIF4G-eIF4A model. Thus, highlighting a possibly compatible interaction axis among eIF3-eIF4G-eIF4A-domain J-K of IRES.

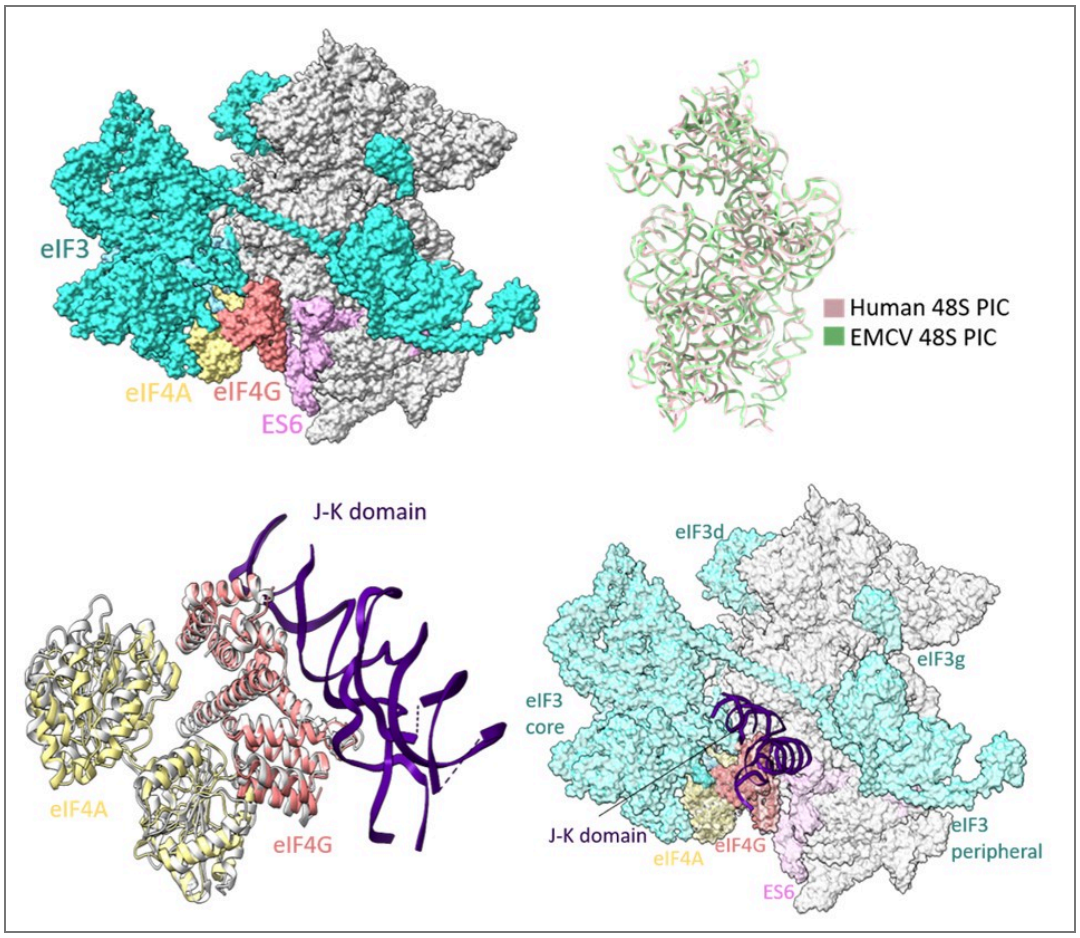

Author response image 7. (upper left) Location of eIF4G-eIF4A in canonical human 48S PIC (PDB Id- 8OZ0). (upper right) Superimposition of 18S rRNA from human 48S and EMCV IRES 48S. (lower left) Superimposition of Human Closed 48S PIC structure (PDB Id- 8OZ0) on EMCV IRES-48S PIC model and placement of EMCV IRES- J-K domain-HEAT1-eIF4A structure (PDB Id- 8HUJ) with respect to eIF4G-HEAT1 domain. (lower right) Predicting location of eIF3 and eIF4 proteins in EMCV IRES-48S PIC.

> *(7) Assuming that the additional density near the ternary complex corresponds to Domain I of the IRES and that the codon in the P site represents the EMCV AUG start codon, what is the authors' mechanistic model for EMCV IRES-mediated initiation? Specifically, how is the mRNA positioned or inserted into the 40S mRNA channel in the absence of canonical scanning? As it stands, the discussion does not sufficiently address this key aspect of the EMCV initiation mechanism.*

The EMCV IRES start codon (A-834) is directly placed in the P site (Pestova et al 1996), and the captured complex harboured the initiator tRNA in P_{IN} state with AUG at the P site. This start codon is preceded by domains J-K-L, where the J-K domain interacts with eIF4 proteins via eIF4G1-HEAT1 domain, and L domain is 20 residues upstream of the AUG and known to interact with eIF4B (Pestova et al 1996; de Quinto et al 2001). Based on the position and binding partners for these domains, the domain L could be placed at the mRNA exit site, preceded by domain J-K, which could be placed close to eIF4G-eIF4A position on EMCV IRES 48S PIC, near expansion segment 6 (ES6). The domain J-K can interact with eIF4G, localized close to the left foot or ES6 as per previous biochemical experiments (Yu et al 2011). This suggests that position of eIF4G and eIF4A could be the same as that of cap-dependent initiation where it can interact with eIF3 core subunits as well as the IRES domain J-K and the predicted path of mRNA from the exit site can follow the path of mRNA in human closed 48S PIC (PDB Id- 8OZ0), where it interacts with eIF3 core.

Examining the path of RNA in channel from the G-825 (exit site) to C-785 (domain J-K), we found the shortest distance is ~ 173 Å. This bridge could be filled by a single-stranded stretch of 40 nucleotides. However, the presence of domain L (stem loop- residues- 782 to 810) might hinder the placement of A-834 in the P-site (Author response image 8). We anticipate that to accommodate the start codon at the P site, either the domain L stem loop is resolved, which is an energetically expensive process (free energy of the thermodynamic ensemble is -11.12 kcal/mol, predicted using RNAfold). Another way could be a change in the orientation or conformation of domain J-K such that the start codon is directly placed at the P site without resolving domain L.

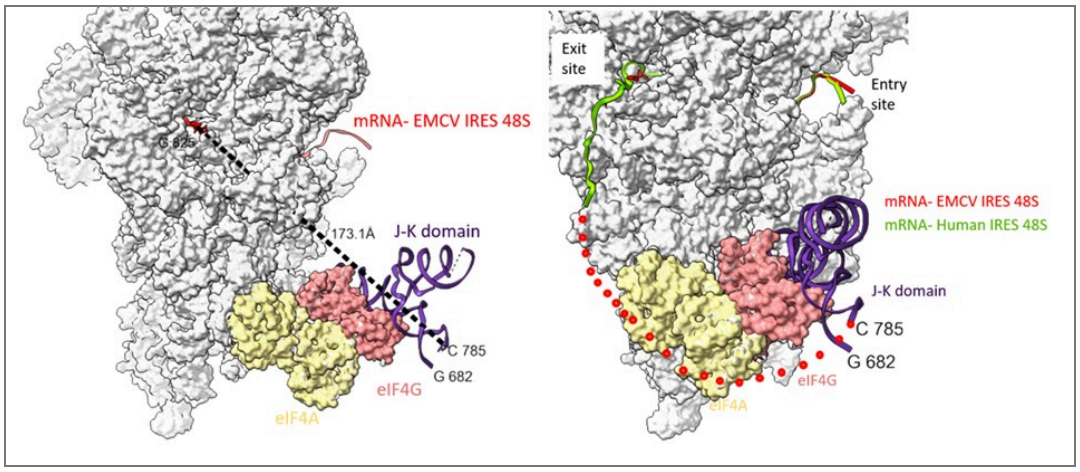

Author response image 8. (left) The shortest distance between the last fitted residue- 825th of EMCV IRES to 785th of J-K domain of IRES (keeping eIF4G position same as that of PDB Id- 8OZ0) is 173 Å. (right) Tracing the path of mRNA (red) upstream of AUG coming out of the exit site of 40S ribosome and the possible position of eIF4G on EMCV IRES-48S PIC. Addition of nucleotides between C-785 and G-825 would fill the gap. The route of predicted mRNA from the exit channel is based on the mRNA (green) exiting the channel (PDB Id- 8OZ0).

The domain I is followed by domain J-K, close to the left foot of the 40S ribosomal subunit as per previous biochemical experiments (Yu et al 2011). However, the minimum distance connecting the I domain at 601st nucleotide to 682nd nucleotide of domain J-K (at the predicted location) is ~300 Å, which might be difficult to be covered by 80 nucleotides (from 601 to 682), present as a double helical strand. We suppose there could be instances of J-K domain repositioning in the EMCV IRES-48S PIC such that the I domain apical region can contact the 40S head and simultaneously place the start codon at the P site (Author response image 9).

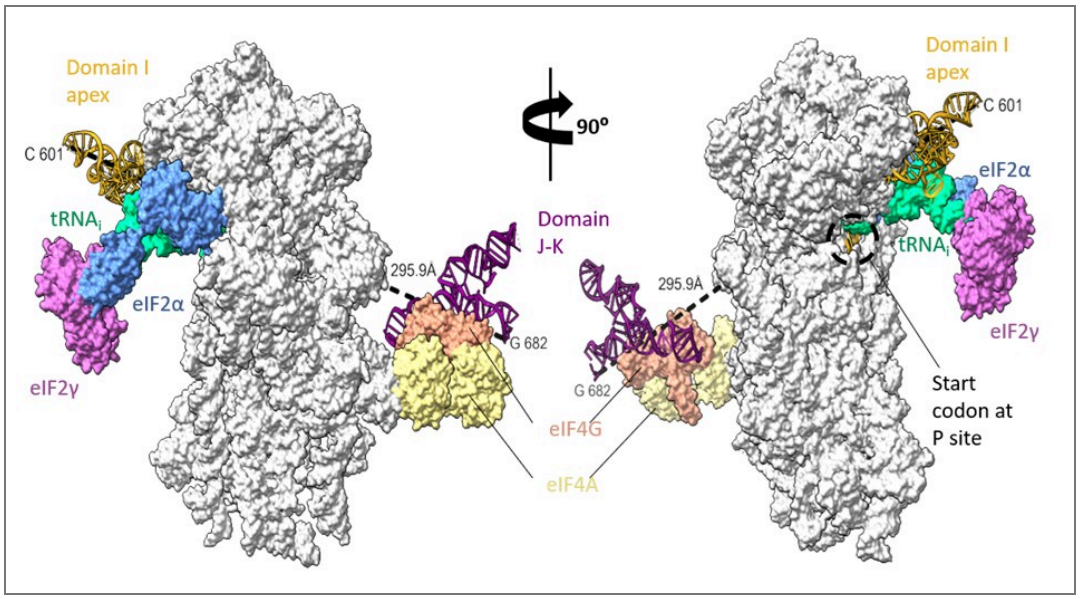

Author response image 9. Rotated views of EMCV IRES domains- I apical part in contact with 40S head and tRNAi and predicted location of J-K domain in contact with eIF4G, close to the left foot of 40S (predicted from PDB Id- 8OZ0). The minimum distance connecting 601st nucleotide in I domain to 682nd nucleotide in J-K domain is 295.5 Å.

We lack any details on the other IRES domains, such as domain I lower stem, domain J-K, or L; therefore, we refrained from commenting on these in our manuscript.

> *(8) Supplementary Figure 1 is missing labels for the RNA ladders.*

The size of the DNA ladder used is mentioned.

References:

Bhattacharjee S, Abaeva IS, Brown ZP, Arhab Y, Fallah H, Hellen CUT, Frank J, Pestova TV. The mechanism of ribosomal recruitment during translation initiation on Type 2 IRESs. bioRxiv [Preprint]. 2025 Jun 11:2025.06.11.659010. doi: 10.1101/2025.06.11.659010. PMID: 40568087; PMCID: PMC12191231.

Brito Querido J, Sokabe M, Díaz-López I, Gordiyenko Y, Fraser CS, Ramakrishnan V. The structure of a human translation initiation complex reveals two independent roles for the helicase eIF4A. Nat Struct Mol Biol. 2024 Mar;31(3):455-464. doi: 10.1038/s41594-023-01196-0. Epub 2024 Jan 29. PMID: 38287194; PMCID: PMC10948362.

Brito Querido J, Sokabe M, Kraatz S, Gordiyenko Y, Skehel JM, Fraser CS, Ramakrishnan V. Structure of a human 48S translational initiation complex. Science. 2020 Sep 4;369(6508):1220-1227. doi: 10.1126/science.aba4904. PMID: 32883864; PMCID: PMC7116333.

Chamond N, Deforges J, Ulryck N, Sargueil B. 40S recruitment in the absence of eIF4G/4A by EMCV IRES refines the model for translation initiation on the archetype of Type II IRESs. Nucleic Acids Res. 2014;42(16):10373-84. doi: 10.1093/nar/gku720. Epub 2014 Aug 26. PMID: 25159618; PMCID: PMC4176346.

Dorn G, Gmeiner C, de Vries T, Dedic E, Novakovic M, Damberger FF, Maris C, Finol E, Sarnowski CP, Kohlbrecher J, Welsh TJ, Bolisetty S, Mezzenga R, Aebersold R, Leitner A, Yulikov M, Jeschke G, Allain FH. Integrative solution structure of PTBP1-IRES complex reveals strong compaction and ordering with residual conformational flexibility. Nat Commun. 2023 Oct 13;14(1):6429. doi: 10.1038/s41467-023-42012-z. PMID: 37833274; PMCID: PMC10576089.

Duke GM, Hoffman MA, Palmenberg AC. Sequence and structural elements that contribute to efficient encephalomyocarditis virus RNA translation. J Virol. 1992 Mar;66(3):1602-9. doi: 10.1128/JVI.66.3.1602-1609.1992. PMID: 1310768; PMCID: PMC240893.

Fernández N, Fernandez-Miragall O, Ramajo J, García-Sacristán A, Bellora N, Eyras E, Briones C, Martínez-Salas E. Structural basis for the biological relevance of the invariant apical stem in IRES-mediated translation. Nucleic Acids Res. 2011 Oct;39(19):8572-85. doi: 10.1093/nar/gkr560. Epub 2011 Jul 8. PMID: 21742761; PMCID: PMC3201876.

Hashem Y, des Georges A, Dhote V, Langlois R, Liao HY, Grassucci RA, Pestova TV, Hellen CU, Frank J. Hepatitis-C-virus-like internal ribosome entry sites displace eIF3 to gain access to the 40S subunit. Nature. 2013 Nov 28;503(7477):539-43. doi: 10.1038/nature12658. Epub 2013 Nov 3. PMID: 24185006; PMCID: PMC4106463.

Imai S, Suzuki H, Fujiyoshi Y, Shimada I. Dynamically regulated two-site interaction of viral RNA to capture host translation initiation factor. Nat Commun. 2023 Aug 28;14(1):4977. doi: 10.1038/s41467-023-40582-6. PMID: 37640715; PMCID: PMC10462655.

Kim H, Kim K, Kwon T, Kim DW, Kim SS, Kim YJ. Secondary structure conservation of the stem-loop IV sub-domain of internal ribosomal entry sites in human rhinovirus clinical isolates. Int J Infect Dis. 2015 Dec;41:21-8. doi: 10.1016/j.ijid.2015.10.015. Epub 2015 Oct 27. PMID: 26518063.

Lomakin IB, Hellen CU, Pestova TV. Physical association of eukaryotic initiation factor 4G (eIF4G) with eIF4A strongly enhances binding of eIF4G to the internal ribosomal entry site of encephalomyocarditis virus and is required for internal initiation of translation. Mol Cell Biol. 2000 Aug;20(16):6019-29. doi: 10.1128/mcb.20.16.6019-6029.2000. PMID: 10913184; PMCID: PMC86078.

López de Quinto S, Martínez-Salas E. Conserved structural motifs located in distal loops of aphthovirus internal ribosome entry site domain 3 are required for internal initiation of translation. J Virol. 1997 May;71(5):4171-5. doi: 10.1128/JVI.71.5.4171-4175.1997. PMID: 9094703; PMCID: PMC191578.

Lozano G, Francisco-Velilla R, Martinez-Salas E. Ribosome-dependent conformational flexibility changes and RNA dynamics of IRES domains revealed by differential SHAPE. Sci Rep. 2018 Apr 3;8(1):5545. doi: 10.1038/s41598-018-23845-x. PMID: 29615727; PMCID: PMC5882922.

Maloney A, Joseph S. Validating the EMCV IRES Secondary Structure with Structure-Function Analysis. Biochemistry. 2024 Jan 2;63(1):107-115. doi: 10.1021/acs.biochem.3c00579. Epub 2023 Dec 11. PMID: 38081770; PMCID: PMC10896073.

Pestova TV, Hellen CU, Shatsky IN. Canonical eukaryotic initiation factors determine initiation of translation by internal ribosomal entry. Mol Cell Biol. 1996 Dec;16(12):6859-69. doi: 10.1128/MCB.16.12.6859. PMID: 8943341; PMCID: PMC231689.

Petrychenko V, Yi SH, Liedtke D, Peng BZ, Rodnina MV, Fischer N. Structural basis for translational control by the human 48S initiation complex. Nat Struct Mol Biol. 2024 Sep 17. doi: 10.1038/s41594-024-01378-4. Epub ahead of print. PMID: 39289545.

Roberts LO, Belsham GJ. Complementation of defective picornavirus internal ribosome entry site (IRES) elements by the coexpression of fragments of the IRES. Virology. 1997 Jan 6;227(1):53-62. doi: 10.1006/viro.1996.8312. PMID: 9007058.

Robertson ME, Seamons RA, Belsham GJ. A selection system for functional internal ribosome entry site (IRES) elements: analysis of the requirement for a conserved GNRA tetraloop in the encephalomyocarditis virus IRES. RNA. 1999 Sep;5(9):1167-79. doi: 10.1017/s1355838299990301. PMID: 10496218; PMCID: PMC1369840.

Sweeney TR, Abaeva IS, Pestova TV, Hellen CU. The mechanism of translation initiation on Type 1 picornavirus IRESs. EMBO J. 2014 Jan 7;33(1):76-92. doi: 10.1002/embj.201386124. Epub 2013 Dec 15. PMID: 24357634; PMCID: PMC3990684.

Velazquez MA, Nuthalapati SS, Hankinson J, Fominykh K, Lulla V, Sweeney TR, Hill CH. Structural and mechanistic insights into translation initiation on the enterovirus Type 1 IRES. bioRxiv [Preprint]. 2025 Oct 3: 2025.10.04.680434. doi: 10.1101/2025.10.04.680434.

Yu Y, Sweeney TR, Kafasla P, Jackson RJ, Pestova TV, Hellen CU. The mechanism of translation initiation on Aichivirus RNA mediated by a novel type of picornavirus IRES. EMBO J. 2011 Aug 26;30(21):4423-36. doi: 10.1038/emboj.2011.306. PMID: 21873976; PMCID: PMC3230369.

https://doi.org/10.7554/eLife.107788.2.sa0